Table 3
Average changes in CBF and MBR after intravenous administration of ET-1.

	Baseline levels	30 min	60 min
CBF (mL/min/100 g)	41.6 ± 10.2	41.9 ± 9.8 (1.02 ± 0.15)	39.4 ± 10.5 (0.95 ± 0.16)
MBR	4.1 ± 0.8	3.9 ± 1.0 (0.95 ± 0.08)	3.9 ± 0.7 (0.95 ± 0.20)

Data are expressed as mean ± SD for 6 rabbits. No significant difference was found. CBF/MBR changes to baseline levels were shown in parentheses.

3.3. Effects of individuality and treatment

Randomized block ANOVA revealed that there were wide ranges of distribution of differences for the basal blood flow measurement and that animals' individuality had significant effects on MBR and CBF (Table 1). Distributions of differences for the time-course changes were relatively narrow. Although the time-course changes in MBR and CBF during ET-1 treatment were not significant, those during CO_2 treatment were significant by repeated measure analysis (Table 1).

Average and individual changes in CBF after treatments are shown in Tables 2 and 3 and Fig. 4, respectively. CBF had a tendency of increasing after CO_2 inhalation (CBF was increased in 6 cases out of 9). ET-1 administration decreased CBF in 5 cases out of 6 though the effect was not significant because CBF was markedly increased in just one case. Representative hydrogen density curve charts are shown in Fig. 5. Average changes in MBR after treatments are shown in Tables 2 and 3. Typical examples of 2-dimensional color-coded MBR maps are shown in Fig. 6.

4. Discussion

This report is the first to verify the correlation of MBR, a new index obtained by CCD-equipped LSFG, with CBF obtained by the hydrogen gas clearance method in the ONH. A significant and positive correlation between the absolute values of CBF and MBR at baseline, as well as their relative changes, was found in the current study. This result suggests that MBR may correlate with CBF and also change with CBF, as an index of blood flow in the ONH, linearly. Since a similar experiment cannot be performed in humans, the present study provides important basal data for the measurement of MBR in humans, though these data cannot be applied directly to humans because of their many histophysiological differences with rabbits.

A power analysis (Correlation: point biserial model) by G* Power software (v. 3.1.3) showed that total sample size of 9 is needed under the condition of effect size of 0.7, error probability (α) of 0.05 and power ($1 - \beta$) of 0.8. Therefore, the sample sizes of 14 and 39 in the current study would be sufficient statistically.

In the present study, inhalation of CO_2 or intravenous administration of ET-1 altered CBF obtained by the hydrogen gas clearance method in rabbit ONH. These results are, at least partly, consistent with previous reports (Sugiyama et al., 1995, 1996). The relative values of CBF and MBR to the initial levels were in the range of 0.74–1.27 and 0.76–1.35, respectively. A significant and positive correlation was also found between the relative changes in CBF and MBR values induced by CO_2 inhalation and ET-1 injection. This correlation suggests that changes in MBR may indicate those in CBF in the ONH. These results appear similar to a previous report (Sugiyama et al., 1996). Though the r value in this study (0.67) was obviously different from that in the previous paper (0.92), the comparison of r values from different experiments does not seem fair since they can be affected by many factors.

In the current study, the r value for the correlation between the absolute values of MBR and CBF was 0.73; this was relatively large and comparable to that between the relative values during CO_2 inhalation and ET-1 injection. This result indicates quantifiability of absolute values of MBR at least under a certain condition. On the other hand, the randomized block ANOVA in the current study revealed significant effects of the individuality of animals on basal values of CBF and MBR. Therefore, care must be taken in interpreting absolute values across individuals, even though the absolute values of MBR were significantly correlated with CBF. In general, measurement results obtained with apparatus that employ lasers are affected by the degree of absorption or reflection of the laser beam in the specific tissue. Particularly in humans, careful interpretation is needed due to relatively large topographical or color differences of the ONH induced by individuality or diseases, which affect absorption and reflection. Actually, we have data on individual variation in MBRs of young normal volunteers; MBRs in the temporal rim were measured in the range of 6.3–13.8 (mean ± SD = 10.6 ± 2.5, n = 9). In addition, MBRs in the nasal

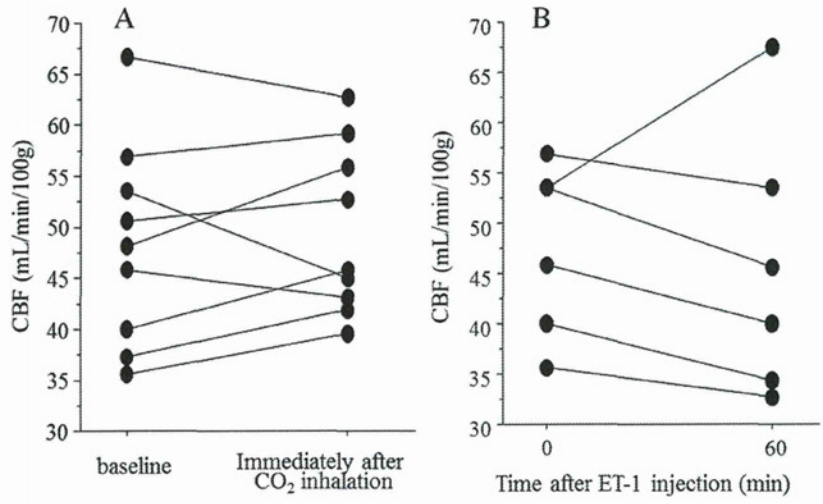

Fig. 4. Individual changes in CBF after 5-min inhalation of 10% CO_2 (A) and administration of 10^{-10} mol/kg ET-1 (B). CBF was increased in 6 cases out of 9, and decreased in 5 cases out of 6 in A and B, respectively.

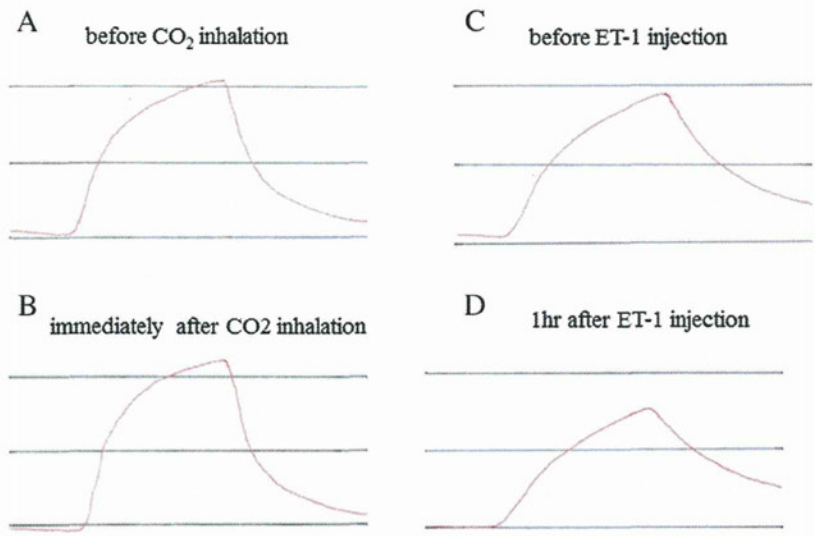

Fig. 5. Representative examples of the hydrogen gas clearance curve. A and B: before and immediately after 5-min inhalation of 10% CO_2 in the same rabbit (A is the same as Fig. 1A). CBF values were 65.3 and 77.6 mL/min/100 g, respectively. C and D: before and 1 h after administration of 10^{-10} mol/kg ET-1 in another same rabbit. CBF values were 40.3 and 32.8 mL/min/100 g, respectively.

rim of them were measured as 17.8 ± 3.9, which are much different from those in the temporal rim. Therefore, the relatively wide range of ONH blood flow in the present study might be due to an individual difference as well as a regional difference.

As a problematic issue for the LSFG apparatus, the zero-offset for MBR was rather large (around 2.5) in the current study. We actually obtained 6.1 and 1.9 as mean values of MBR ($n = 2$) at the same spot of ONH just before and shortly after a rabbit was euthanized (the hydrogen gas clearance method cannot be available while it is dead because inhalation is impossible then) in the additional experiment. This result (mean value of MBR was 1.9 when blood flow was stopped in dead rabbits) is almost consistent with the zero-offset of approximately 2.5. In addition, since a range of baseline values of MBR was 3.5–6.0, the ratio of the highest to the lowest (6.0/3.5) was smaller than those by the hydrogen gas clearance method (83.5/32.4). Taken together, there seems to be a room for more

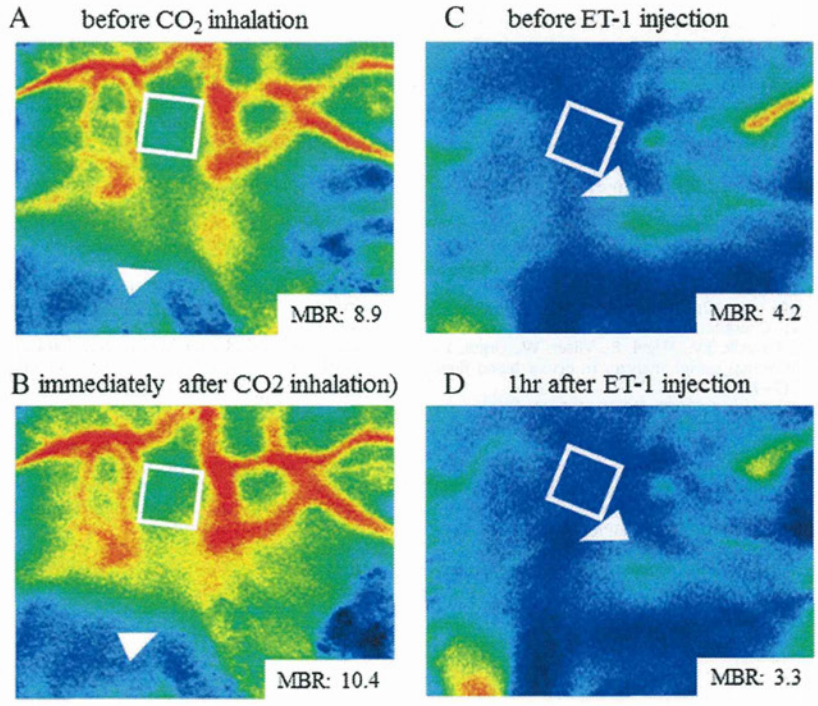

Fig. 6. Representative examples of color-coded MBR maps obtained by LSFG. A and B: before and immediately after 5-min inhalation of 10% CO_2 in the same rabbit. C and D: before and 1 h after administration of 10^{-10} mol/kg ET-1 in another rabbit. Arrowheads indicate the tips of electrodes for the hydrogen gas clearance method, and white squares indicate the areas analyzed by LSFG.

adequate calibration of MBR values. While these results (a relatively large zero-offset and a smaller relative change in MBR) were only for the animal model in the current study. Further investigation using other animals should also be needed in the future for validation of quantifiability of measurement of ONH microcirculation by LSFG.

Many agents have been reported to alter ocular blood flow (Araie and Mayama, 2011; Shimazawa et al., 1999; Sugiyama and Azuma, 1995; Sugiyama et al., 2010, 2011; Tokushige et al., 2011; Waki et al., 2001). Since the present study revealed that MBR may correlate with tissue blood flow in the ONH, LSFG-NAVI™ will likely provide new relevant information concerning the ONH blood flow in glaucoma and support in verifying whether increasing ONH blood flow could be a promising strategy for glaucoma management.

5. Conclusions

Our results suggest that MBR obtained by CCD-equipped LSFG may correlate with CBF and also change with CBF, as an index of blood flow in the ONH, linearly.

Financial disclosure

H. Takahashi and H. Tokushige are employees of Senju Pharmaceutical Co., Ltd. The other authors have no financial disclosures.

Acknowledgments

The authors thank Y.T. for her technical support and kindest encouragement, Mr. Mitsunori Waki for his technical advice and valuable discussions, and Dr. Tomoyuki Wada for his advice concerning statistics and his encouragement.

References

Aizawa, N., Yokoyama, Y., Chiba, N., Omodaka, K., Yasuda, M., Otomo, T., Nakamura, M., Fuse, N., Nakazawa, T., 2011. Reproducibility of retinal circulation measurements obtained using laser speckle flowgraphy-NAVI in patients with glaucoma. Clin. Ophthalmol. 5, 1171–1176.

Araie, M., Mayama, C., 2011. Use of calcium channel blockers for glaucoma. Prog. Retin. Eye Res. 30, 54–71.

Aukland, K., Bower, B.F., Berliner, R.W., 1964. Measurement of local blood flow with hydrogen gas. Circ. Res. 14, 164–187.

Caprioli, J., Coleman, A.L., 2010. Blood pressure, perfusion pressure, and glaucoma. Am. J. Ophthalmol. 149, 704–712.

Csete, K., Vezekényi, Z., Dóczi, T., Papp, J.G., Bodosi, M., Barzó, P., 2004. Comparison of regional vasomotor responses to acetazolamide and CO_2 in rabbit cerebrum and cerebellum, measured by a hydrogen clearance method. Acta Physiol. Scand. 182, 287–294.

Ernest, J.T., 1976. Optic disc blood flow. Trans. Ophthalmol. Soc. U.K. 96, 348–351.

Garhofer, G., Bek, T., Boehm, A.G., Gherghel, D., Grunwald, J., Jeppesen, P., Kergoat, H., Kotliar, K., Lanzl, I., Lovasik, J.V., Nagel, E., Vilser, W., Orgul, S., Schmetterer, L., 2010. Use of the retinal vessel analyzer in ocular blood flow research. Acta Ophthalmol. 88, 717–722.

Grieshaber, M.C., Mozaffarieh, M., Flammer, J., 2007. What is the link between vascular dysregulation and glaucoma? Surv. Ophthalmol. 52 (Suppl. 2), S144–S154.

Harris, A., Kagemann, L., Ehrlich, R., Rospigliosi, C., Moore, D., Siesky, B., 2008a. Measuring and interpreting ocular blood flow and metabolism in glaucoma. Can. J. Ophthalmol. 43, 328–336.

Harris, A., Werne, A., Cantor, L.B., 2008b. Vascular abnormalities in glaucoma: from population-based studies to the clinic? Am. J. Ophthalmol. 145, 595–597.

Konishi, N., Tokimoto, Y., Kohra, K., Fujii, H., 2002. New laser speckle flowgraphy system using CCD camera. Opt. Rev. 9, 163–169.

Logan, J.F., Rankin, S.J., Jackson, A.J., 2004. Retinal blood flow measurements and neuroretinal rim damage in glaucoma. Br. J. Ophthalmol. 88, 1049–1054.

Moore, D., Harris, A., Wudunn, D., Kheradiya, N., Siesky, B., 2008. Dysfunctional regulation of ocular blood flow: a risk factor for glaucoma? Clin. Ophthalmol. 2, 849–861.

Nagahara, M., Tamaki, Y., Araie, M., Fujii, H., 1999. Real-time blood velocity measurements in human retinal vein using the laser speckle phenomenon. Jpn. J. Ophthalmol. 43, 186–195.

Pemp, B., Georgopoulos, M., Vass, C., Fuchsjager-Mayrl, G., Luksch, A., Rainer, G., Schmetterer, L., 2009. Diurnal fluctuation of ocular blood flow parameters in patients with primary open-angle glaucoma and healthy subjects. Br. J. Ophthalmol. 93, 486–491.

Riva, C.E., Geiser, M., Petrig, B.L., 2010. Ocular blood flow assessment using continuous laser doppler flowmetry. Acta Ophthalmol. 88, 622–629.

Shimazawa, M., Sugiyama, T., Azuma, I., Araie, M., Iwakura, Y., Watari, M., Sakai, T., Hara, H., 1999. Effect of lomerizine, a new Ca^{2+}channel blocker, on the microcirculation in the optic nerve head in conscious rabbits: a study using a laser speckle technique. Exp. Eye Res. 69, 185–193.

Srinivasan, V.J., Atochin, D.N., Radhakrishnan, H., Jiang, J.Y., Ruvinskaya, S., Wu, W., Barry, S., Cable, A.E., Ayata, C., Huang, P.L., Boas, D.A., 2011. Optical coherence tomography for the quantitative study of cerebrovascular physiology. J. Cereb. Blood Flow Metab. 31, 1339–1345.

Stalmans, I., Vandewalle, E., Anderson, D.R., Costa, V.P., Frenkel, R.E., Garhofer, G., Grunwald, J., Gugleta, K., Harris, A., Hudson, C., Januleviciene, I., Kagemann, L., Kergoat, H., Lovasik, J.V., Lanzl, I., Martinez, A., Nguyen, Q.D., Plange, N., Reitsamer, H.A., Sehi, M., Siesky, B., Zeitz, O., Orgul, S., Schmetterer, L., 2011. Use of colour doppler imaging in ocular blood flow research. Acta Ophthalmol. 89, e609–630.

Sugiyama, T., Araie, M., Riva, C.E., Schmetterer, L., Orgul, S., 2010. Use of laser speckle flowgraphy in ocular blood flow research. Acta Ophthalmol. 88, 723–729.

Sugiyama, T., Azuma, I., 1995. Effect of UF-021 on optic nerve head circulation in rabbits. Jpn. J. Ophthalmol. 39, 124–129.

Sugiyama, T., Moriya, S., Oku, H., Azuma, I., 1995. Association of endothelin-1 with normal tension glaucoma: clinical and fundamental studies. Surv. Ophthalmol. 39 (Suppl. 1), S49–S56.

Sugiyama, T., Shibata, M., Kajiura, S., Okuno, T., Tonari, M., Oku, H., Ikeda, T., 2011. Effects of fasudil, a rho-associated protein kinase inhibitor, on optic nerve head blood flow in rabbits. Invest. Ophthalmol. Vis. Sci. 52, 64–69.

Sugiyama, T., Utsumi, T., Azuma, I., Fujii, H., 1996. Measurement of optic nerve head circulation: comparison of laser speckle and hydrogen clearance methods. Jpn. J. Ophthalmol. 40, 339–343.

Takayama, J., Tomidokoro, A., Ishii, K., Tamaki, Y., Fukaya, Y., Hosokawa, T., Araie, M., 2003. Time course of the change in optic nerve head circulation after an acute increase in intraocular pressure. Invest. Ophthalmol. Vis. Sci. 44, 3977–3985.

Tamaki, Y., Araie, M., Fukaya, Y., Nagahara, M., Imamura, A., Honda, M., Obata, R., Tomita, K., 2003. Effects of lomerizine, a calcium channel antagonist, on retinal and optic nerve head circulation in rabbits and humans. Invest. Ophthalmol. Vis. Sci. 44, 4864–4871.

Tamaki, Y., Araie, M., Kawamoto, E., Eguchi, S., Fujii, H., 1995. Non-contact, two-dimensional measurement of tissue circulation in choroid and optic nerve head using laser speckle phenomenon. Exp. Eye Res. 60, 373–383.

Tamaki, Y., Araie, M., Kawamoto, E., Eguchi, S., Fujii, H., 1994. Noncontact, two-dimensional measurement of retinal microcirculation using laser speckle phenomenon. Invest. Ophthalmol. Vis. Sci. 35, 3825–3834.

Tamaki, Y., Araie, M., Tomita, K., Tomidokoro, A., 1996. Time change of nicardipine effect on choroidal circulation in rabbit eyes. Curr. Eye Res. 15, 543–548.

Tokushige, H., Waki, M., Takayama, Y., Tanihara, H., 2011. Effects of Y-39983, a selective rho-associated protein kinase inhibitor, on blood flow in optic nerve head in rabbits and axonal regeneration of retinal ganglion cells in rats. Curr. Eye Res. 36, 964–970.

Tomidokoro, A., Araie, M., Tamaki, Y., Tomita, K., 1998. In vivo measurement of iridial circulation using laser speckle phenomenon. Invest. Ophthalmol. Vis. Sci. 39, 364–371.

Tomita, K., Araie, M., Tamaki, Y., Nagahara, M., Sugiyama, T., 1999. Effects of nilvadipine, a calcium antagonist, on rabbit ocular circulation and optic nerve head circulation in NTG subjects. Invest. Ophthalmol. Vis. Sci. 40, 1144–1151.

Waki, M., Sugiyama, T., Watanabe, N., Ogawa, T., Shirahase, H., Azuma, I., 2001. Effect of topically applied iganidipine dihydrochloride, a novel calcium antagonist, on optic nerve head circulation in rabbits. Jpn. J. Ophthalmol. 45, 76–83.

Watanabe, G., Fujii, H., Kishi, S., 2008. Imaging of choroidal hemodynamics in eyes with polypoidal choroidal vasculopathy using laser speckle phenomenon. Jpn. J. Ophthalmol. 52, 175–181.

Yamazaki, Y., Drance, S.M., 1997. The relationship between progression of visual field defects and retrobulbar circulation in patients with glaucoma. Am. J. Ophthalmol. 124, 287–295.

The American Journal of Pathology, Vol. 181, No. 1, July 2012

http://dx.doi.org/10.1016/j.ajpath.2012.03.022

Cell Injury, Repair, Aging, and Apoptosis

The Regulatory Roles of Apoptosis-Inducing Factor in the Formation and Regression Processes of Ocular Neovascularization

Toshio Hisatomi,*†‡ Shintaro Nakao,*† Yusuke Murakami,*† Kousuke Noda,* Toru Nakazawa,* Shoji Notomi,† Edward Connolly,* Haicheng She,* Lama Almulki,* Yasuhiro Ito,* Demetrios G. Vavvas,* Tatsuro Ishibashi,† and Joan W. Miller*

From the Angiogenesis Laboratory, Massachusetts Eye and Ear Infirmary, Department of Ophthalmology, Harvard Medical School, Boston, Massachusetts; the Department of Ophthalmology,† Graduate School of Medical Sciences, Kyushu University, Fukuoka, Japan; and the Clinical Research Institute,‡ Kyushu Medical Center, Fukuoka, Japan*

The role of apoptosis in the formation and regression of neovascularization is largely hypothesized, although the detailed mechanism remains unclear. Inflammatory cells and endothelial cells both participate and interact during neovascularization. During the early stage, these cells may migrate into an angiogenic site and form a pro-angiogenic microenvironment. Some angiogenic vessels appear to regress, whereas some vessels mature and remain. The control mechanisms of these processes, however, remain unknown. Previously, we reported that the prevention of mitochondrial apoptosis contributed to cellular survival via the prevention of the release of pro-apoptotic factors, such as apoptosis-inducing factor (AIF) and cytochrome *c*. In this study, we investigated the regulatory role of cellular apoptosis in angiogenesis using two models of ocular neovascularization: laser injury choroidal neovascularization and VEGF-induced corneal neovascularization in AIF-deficient mice. Averting apoptosis in AIF-deficient mice decreased apoptosis of leukocytes and endothelial cells compared to wild-type mice and resulted in the persistence of these cells at angiogenic sites *in vitro* and *in vivo*. Consequently, AIF deficiency expanded neovascularization and diminished vessel regression in these two models. We also observed that peritoneal macrophages from AIF-deficient mice showed anti-apoptotic survival compared to wild-type mice under conditions of starvation. Our data suggest that AIF-related apoptosis plays an important role in neovascularization and that mitochondria-regulated apoptosis could offer a new target for the treatment of pathological angiogenesis. *(Am J Pathol 2012, 181:53–61; http://dx.doi.org/10.1016/j.ajpath.2012.03.022)*

The mitochondrial apoptosis pathways are important mechanisms of cell death.[1] Mitochondria contain pro-apoptotic factors such as cytochrome *c* and apoptosis-inducing factor (AIF) in their intermembrane space. Furthermore, mitochondrial outer membrane permeabilization is a critical event during apoptosis, representing the "point of no return" of the lethal process. Cytochrome *c* is released from mitochondria on mitochondrial outer membrane permeabilization and binds to cytosolic apoptotic protease activating factor-1 to induce its dimerization and a conformational change.[2] Apoptotic protease activating factor-1 then oligomerizes into apoptosomes that recruit and activate caspase-9 followed by serial activation of apoptosis-execution molecules.[3,4] Mitochondrial outer membrane permeabilization, however, may cause cell death even if caspases are inhibited[5] and a broad caspase inhibitor (z-VAD-fmk) fails to block apoptosis in retinal neurons.[6] AIF is a caspase-independent apoptogenic factor and is normally confined to the mitochondrial intermembrane space.[7] Most cell death in vertebrates proceeds via the mitochondrial pathway of apoptosis, especially in mammalian cells.[8,9] During

Supported by an Alcon Research Award (J.W.M.), Japan Eye Bank Association (T.H.), a Bausch & Lomb Vitreoretinal Fellowship (T.N.), and National Eye Institute Grant EY014104 (Massachusetts Eye and Ear Infirmary Core Grant).

Accepted for publication March 15, 2012.

T.H., S.N., and Y.M. contributed equally to this work.

Address reprint requests to Joan W. Miller, M.D., Massachusetts Eye and Ear Infirmary, 243 Charles St., Boston, MA 02114, or Tatsuro Ishibashi, M.D., Ph.D., Department of Ophthalmology, Graduate School of Medical Sciences, Kyushu University, 3-1-1 Maidashi Higashi-ku, Fukuoka, 812-8582, Japan. E-mail: Joan_Miller@meei.harvard.edu or ishi@eye.med.kyushu-u.ac.jp.

apoptosis, AIF translocates to the cytosol and then to the nucleus where it triggers peripheral chromatin condensation and interacts with cyclophilin A to generate a DNase complex, which is responsible for the so-called "large-scale" DNA degradation to fragments of approximately 50 kbp.[10] AIF is strongly conserved among mammalian species (>95% amino acid identity between mouse and human) and bears a highly significant homology with flavoprotein oxidoreductases from all eukaryotic and prokaryotic kingdoms in its C-terminal portion.[7] Because AIF, a central player in mitochondrial apoptotic pathways is essential in the developmental process, AIF knockout mice die *in utero*.[11] Based on these findings, it is reasonable to speculate that AIF may be a phylogenetically old major mediator participating in various aspects of the apoptotic process. Because we originally reported AIF translocation in mammalian cells *in vivo* in retinal cell death,[6,9,12–16] the translocation of AIF has been reported in neurodegeneration[17,18] and retinal degeneration.[19] The contribution of apoptosis, especially phylogenetically old major factors (ie, AIF), however, has remained elusive in the field of neovascularization.

Choroidal neovascularization (CNV) is a pathological process involving the formation of new blood vessels from choroidal vasculature through Bruch's membrane breaks. CNV is associated with a variety of ocular diseases, including age-related macular degeneration (AMD), myopia, histoplasmosis, angioid streaks, tumors, and traumatic and idiopathic conditions, all of which often cause severe visual loss via retinal degeneration. CNV could be induced by focally increased inflammatory and proangiogenic factors, and/or by a decrease of anti-angiogenic factors. Various clinical, as well as experimental, studies have shown that vascular endothelial growth factor (VEGF)-A could be the most important factor for CNV.[20] Recent observations in age-related macular degeneration patients with VEGF-A inhibition strongly support the importance in CNV. In CNV, macrophages may be major sources of VEGF-A, which would enhance vascular leakage, as well as angiogenesis via vascular endothelial growth factor receptor (VEGFR)-2.[21] Macrophage also expresses VEGFR-1 and VEGF-A that may induce macrophage infiltration. Thus, VEGF is an inflammatory cytokine targeting both leukocytes and endothelial cells. Various studies have shown attachment of mural cells is important for the vascular stability that is dependent on angiopoietin/Tie system and VEGF.[22] Tie2 is known to play a direct role in pericyte recruitment and Tie2-knockout blood vessels that lack mural cells.[23] The loss of periendothelial cells in the mutants is secondary to endothelial cell apoptosis.[24]

The efficient clearance of excessive inflammatory cells and neovascular endothelial cells from the pathological sites may be essential for restoration of tissue homeostasis.[13] The regulation of apoptosis in angiogenesis-related cells, including leukocytes and endothelial cells, may occur in various disorders. The detailed mechanism, however, remains unclear.[25] In this study, we focused on the roles of a major proapoptotic molecule, AIF in the formation and regression of neovascularization.

Materials and Methods

Experimental Animals

All animal procedures were performed in accordance with the statement of the Association for Research in Vision and Ophthalmology and the protocol approved by the Animal Care Committee of Massachusetts Eye and Ear Infirmary. The AIF mutant mice (B6CBACa Aw-J/A-Aifm1Hq/J, stock number 000501; Jackson Laboratory, Bar Harbor, ME) and wild type (WT) from the colony were purchased from the Jackson Laboratory and bred in our laboratory. Adult male mice (8 weeks of age) were used for the following experiments.

Laser Injury-Induced Choroidal Neovascularization

Mice were anesthetized with ketamine (100 mg/kg) and xylazine (10 mg/kg). Pupils were dilated with 5.0% phenylephrine and 0.8% tropicamide. CNV was induced with a 532 nm laser (Oculight GLx, Iridex, Mountain View, CA) as previously described.[20,26–31] Four laser spots (150 mW, 100 msec, 50 μm settings) were placed in each eye using a slit-lamp delivery system and a cover glass as a contact lens (n = 16 for each time point and strain). Production of a bubble at the time of laser confirmed the rupture of the Bruch's membrane. The vessels were stained with fluorescein isothiocyanate-dextran. The eyes were enucleated at 2, 4, and 12 weeks after laser injury and fixed in 4% paraformaldehyde for 3 hours. The anterior segment and retina were removed from the eyecup. Approximately four to six relaxing radial incisions were made, and the remaining retinal pigment epithelial-choroidal-scleral complex was flat mounted and coverslipped. Pictures of the choroidal flat mounts were taken, and Openlab software version 5 (Improvision, Boston, MA) was used to measure the hyperfluorescent areas corresponding to the CNV lesions. The average size of the CNV lesions was then determined and used for the evaluation.

Bone Marrow Transplantation

To characterize the angiogenic roles of infiltrating macrophages, we produced chimera green fluorescent protein (GFP) mice, by a previously described method.[13,32] Briefly, we used the transgenic mouse as a cell source for enhanced GFP (EGFP)-positive bone marrow cells. The host mice took 1,4-butanediol dimethanesulfonate, Busulfan 4 × 25 mg/kg on 4 consecutive days followed by bone marrow transplantation (BMT) to deplete stem cells in the host and consequently allow for high levels of long-term, donor-type engraftment. A successful bone marrow transplantation was confirmed by the identification of GFP-positive cells in the blood at 2 and 4 weeks after BMT. The WT and AIF-deficient mice took BMT from EGFP transgenic mice and laser injury 4 weeks after BMT (n = 10, each group). The eyes were harvested and examined 2 weeks after laser injury, as previously described. To visualize EGFP-positive macrophage in the CNV, the vessels were stained with rhodamine-conjugated concanavalin A.

Corneal Micropocket Assay in Mice

Mice were anesthetized with ketamine (100 mg/kg) and xylazine (10 mg/kg). Poly 2-hydroxyethyl methacrylate pellets (0.3 μL, P3932; Sigma-Aldrich, St. Louis, MO) containing 200 ng VEGF-A (293-VE; R&D Systems, Minneapolis, MN) were prepared and implanted into the corneas. VEGF-A pellets were positioned at approximately 1 mm distant to the corneal limbus. After implantation, bacitracin ophthalmic ointment (E. Fougera & Co., Melville, NY) was applied to each eye to prevent infection. At 6 days (n = 6, each group), 10 days (n = 8), 14 days (n = 10), 28 days (n = 8), 56 days (n = 10), 84 days (n = 5), and 140 days (n = 3) after implantation, digital images of the corneal vessels were obtained and recorded using OpenLab software version (Improvision Inc., Lexington, MA) with standardized illumination and contrast. The quantitative analysis of neovascularization in the mouse corneas was performed using Scion Image software (version 4.0.2; Scion Corp., Frederick, MD).

TUNEL Assay

TUNEL and quantification of TUNEL$^+$ cells were performed as previously described,[6] using the ApopTag Fluorescein *in Situ* Apoptosis Detection Kit (Chemicon/Millipore, Bedford, MA). The center of the choroidal and corneal neovascularization was photographed, and the number of TUNEL$^+$ cells in the microscopic field was counted in a masked fashion. The results are presented as the mean ± SD.

Immunohistochemistry

The eyes were harvested and snap-frozen in optimal cutting temperature compound (Sakura Finetechnical). Sections (10 μm) were prepared, air dried, and fixed in ice-cold acetone for 10 minutes. The sections were blocked with 3% nonfat dried milk bovine working solution (M7409; Sigma-Aldrich) and stained with a macrophage marker, anti-mouse CD11b (1:50, BD Pharmingen, San Diego, CA) or an endothelial marker, anti-mouse CD31 mAb (1:50; BD Pharmingen), a myeloid lineage marker, CD45 (1:100, BD Pharmingen), VEGF, TNF-α (1:100, Santa Cruz Biotechnology, Santa Cruz, CA), basic fibroblast growth factor, IL-1β (Abcam, Cambridge, MA), and rabbit anti-AIF (1:50, R&D Systems).[33] After an overnight incubation, sections were washed and stained for 40 minutes with Alexa Fluor488 goat anti-rat IgG (20 μg/mL, A11006; Invitrogen). The specimens were observed with a fluorescent microscope and confocal microscope (Nikon, Tokyo, Japan).

Transmission Electron Microscopy

The eyes were enucleated and the posterior segments were fixed in 2.5% glutaraldehyde and 2% paraformaldehyde in 0.1 mol/L cacodylate buffer with 0.08 mol/L $CaCl_2$ at 4°C. The specimens were postfixed for 1.5 hours in 2% aqueous OsO_4, dehydrated in ethanol and water, and embedded in Epon (Electron Microscopy Sciences, Hatfield, PA). Ultrathin sections were cut from blocks and stained with saturated, aqueous uranyl acetate and Sato's lead stain. The specimens were observed with a Hitachi H-7650 electron microscope.

Fluorescein Angiography in CNV Model

Fluorescein angiography was performed by an operator masked to the genetic identity of the animal, with a commercial camera and imaging system (TRC 50 VT camera and IMAGEnet 1.53 system; Topcon, Paramus, NJ), at 2 weeks after laser photocoagulation (WT mice; n = 12, AIF-deficient mice; n = 12). The photographs were captured with a 20-dimensional lens in contact with the fundus camera lens, after intraperitoneal injection of 0.1 mL of 1% fluorescein sodium (Akorn, Decatur, IL). Two masked retina specialists evaluated the fluorescein angiograms at a single sitting. Lesions were graded on an ordinal scale based on the spatial and temporal evolution of fluorescein leakage as follows: grade 0 (nonleaky): no leakage, faint hyperfluorescence, or mottled fluorescence without leakage; grade1 (questionable leakage): hyperfluorescent lesion without progressive increase in size or intensity; grade 2A (leaky): hyperfluorescence increasing in intensity but not in size, no definite leakage; grade 2B (pathologically significant leakage): hyperfluorescence increasing in intensity and in size, definite leakage.[34]

Macrophage Culture from AIF-Deficient Mice

Briefly, peritoneal macrophages were collected by a previously described method.[14,35,36] Peritoneal macrophages were stimulated by injecting Thioglycollate medium into the mouse peritoneal space and collected by washing peritoneal space with 5 mL PBS. Cell density was adjusted to 3.5×10^4 cells each well of an 8-well chamber (Nunc, Thermo Fisher Scientific, Rochester, NY) with Dulbecco's modified Eagle's medium supplemented with 10% fetal bovine serum. We counted the number of TUNEL$^+$ apoptotic macrophages in the culture before and after starvation. For starvation, cells were cultured in Dulbecco's modified Eagle's medium without fetal bovine serum supplement and incubated for 24 hours. The number of TUNEL$^+$ apoptotic macrophages was counted in 10 random fields per well in a masked fashion using ImageJ software version 1.38x (NIH, Bethesda, MD) in Harlequin (Hq) and WT mice. Values are given as the mean ± SEM of 10 replicate wells.

Statistical Analysis

The data from the TUNEL and *in vitro* survival assays were analyzed with the Scheffé post hoc test using StatView 4.11J software for Macintosh (Abacus Concepts Inc., Berkeley, CA). Significance level was set at $P < 0.05$ and $P < 0.01$. The data represent mean ± SD, except for primary culture results.

Results

Nuclear AIF Translocation in TUNEL$^+$ Apoptotic Cells in the Mouse Choroidal Neovascularization

Laser injury-induced neovascular tissue formation from the choroid beneath the retina in 2 weeks in the WT mouse (Figure 1A). TUNEL$^+$ apoptotic cells were ob-

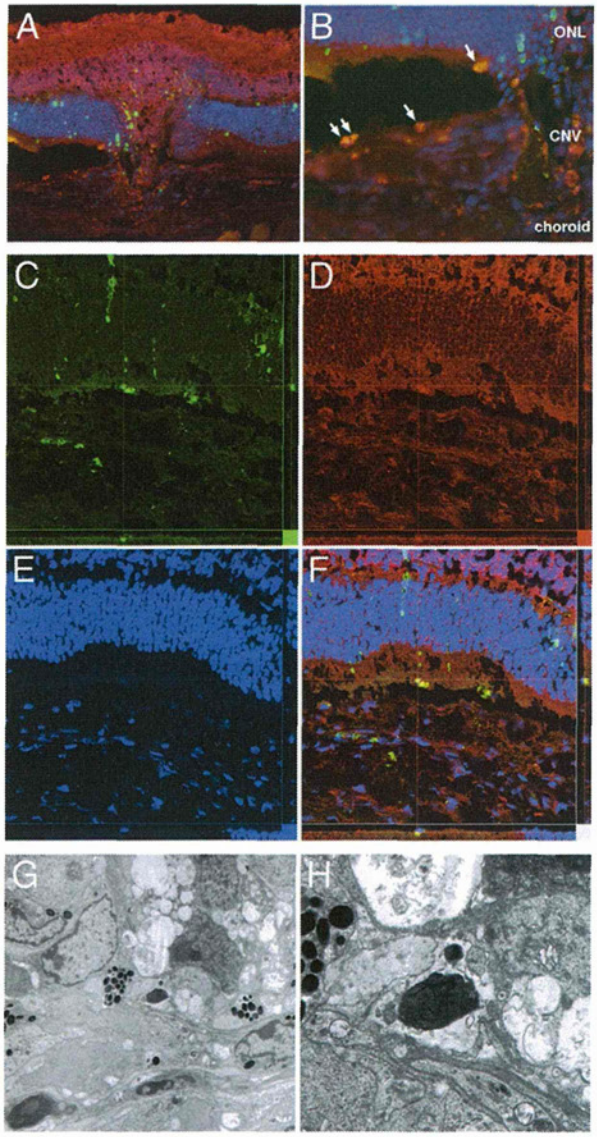

Figure 1. A: Apoptotic cell death and mitochondrio-nuclear translocation of AIF in choroidal neovascularization (CNV). The CNV developed from choroidal tissue into the subretinal space in the WT mouse. **B:** Abundant TUNEL$^+$ cells are observed in the CNV (green), and these cells also showed nuclear accumulation of AIF (red). In contrast, diffuse weak staining of AIF is observed in the cytosol of the nonapoptotic normal cells. **C–F:** Confocal microscopy also confirms co-localization of TUNEL (**C**) and AIF (**D**) in high resolution images. Nuclei are stained blue (**E**); merge is also shown (**F**). **G** and **H:** The electron microscopy shows the morphological characteristics of cellular apoptosis, namely chromatin condensation, cellular shrinkage, and apoptotic body formation in the CNV. Original magnification: ×200 (**A**); ×400 (**B–F**); ×750 (**G**) and ×2500 (**H**). ONL, outer nuclear layer.

served in the retina, subretinal space, and choroidal neovascularization. Nuclear translocation (accumulation) of AIF was abundantly observed in TUNEL$^+$ apoptotic cells in the subretinal space and the choroid (Figure 1B). In contrast, AIF is diffusely noted in the cytosol of the nonapoptotic normal cells. Confocal microscopy also confirmed co-localization of TUNEL and AIF in high resolution images (Figure 1, C–F). The electron microscopy showed the morphological characteristics of cellular apoptosis, namely chromatin condensation, cellular shrinkage, and apoptotic body formation (Figure 1, G and H).

AIF Deficiency Promotes CNV Expansion and Retards Regression

Hq mice exhibit an X chromosome-linked ataxia due to the progressive degeneration of terminally differentiated cerebellar neurons.[37,38] The Hq mutation has been identified as a proviral insertion in the apoptosis-inducing factor (*Aif*) gene (alias programmed cell death 8, *Pdcd8*), causing approximately an 80% reduction in AIF expression.[38] In contrast to Aif knockout mice, which die *in utero*,[11] Hq mice are born at normal Mendelian ratios and are healthy until the age of 3 months.

Laser-induced CNV in AIF-deficient mice led to lesions 1.7-fold larger than WT 2 weeks after laser (Figure 2, A–C). CNV also continues to grow in size in Hq mice to 4 weeks after laser, in contrast to WT mice (Figure 2C). CNV typically regresses rapidly in WT mice, but persists in Hq mice to 12 weeks. To test the regulatory roles of infiltrating macrophage in the CNV progression, we transplanted bone marrow cells from EGFP transgenic wt mice into WT and AIF-deficient mice 4 weeks before the laser injury (Figure 2, D

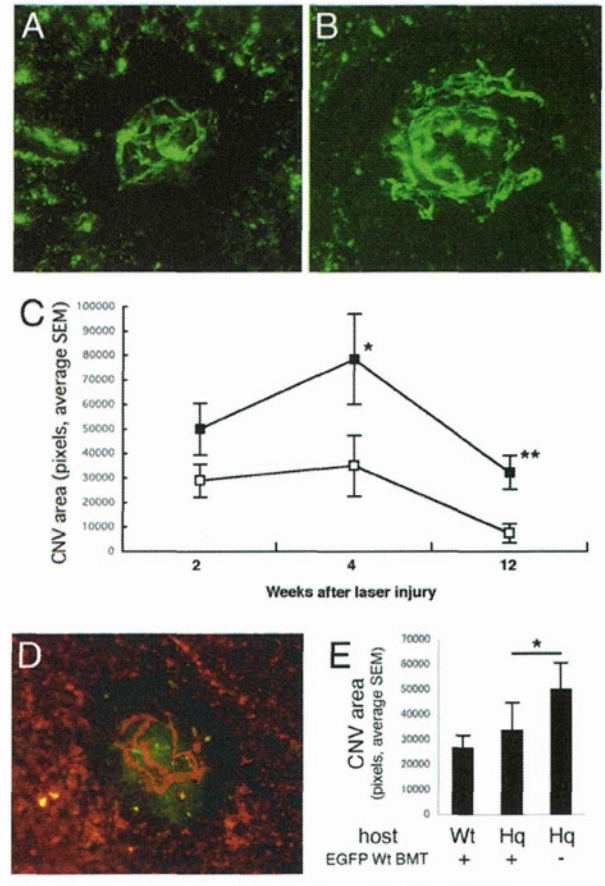

Figure 2. Choroidal neovascularization observed by choroidal flat mount. CNV is visualized with fluorescent injection and analyzed with analysis software. AIF-deficient mice (**B**) induce larger CNV formation than normal WT mice (**A**). **C:** Even after 12 weeks AIF-deficient mice (black box) show persistent CNV, whereas WT mice (white box) show regression of formed CNV. **D:** The EGFP-positive WT macrophages reconstructed from transplanted bone marrow migrate in the CNV stained with rhodamine conjugated concanavalin A. **E:** The CNV size increased in AIF-deficient mice compared to WT mice; conversely, CNV size was decreased in AIF-deficient mice with WT bone marrow transplantation. $^*P < 0.05$, $^{**}P < 0.01$. Hq, Harlequin.

and E). The EGFP-positive WT macrophages reconstructed from transplanted bone marrow migrated in the CNV (Figure 2D). The CNV size increased in AIF-deficient mice compared to WT mice, whereas the size was decreased in reverse in the AIF-deficient mice with WT bone marrow transplantation (Figure 2E). These experiments support that AIF deficiency resulted in enlarged CNV, which continued to grow and exhibited less regression relative to WT mice.

AIF Deficiency Decreases Apoptosis of Infiltrating Macrophages and Neovascular Endothelial Cells in CNV

Vertical histological sections also showed a large area of CNV in Hq mice in contrast to WT mice (Figure 3A). A large number of CD45-positive myeloid lineage cells migrated in the laser injury area and accumulated in the CNV. CD11b-positive macrophages were also present in CNV lesions (Figure 3B). In WT mice, $TUNEL^+$ apoptotic cells were abundant among CD11b(+) macrophages and CD31(+) endothelial cells. AIF-deficient mice, however, showed fewer $TUNEL^+$ apoptotic cells in the CNV. To test the roles of CD11b-positive macrophages, immunohistochemistry of CD11b and four major angiogenic or inflammatory factors, namely VEGF, TNF-α, basic fibroblast growth factor, and IL-1β, was examined in the CNV (Figure 3C). These four factors were expressed in CD11b positive macrophages. VEGF was strongly expressed in neovascular tissue, especially in the macrophages. These data suggest that AIF deficiency enhanced macrophage accumulation and angiogenic factor expression in the CNV.

AIF Deficiency Promotes CNV Leakage on Fluorescein Angiography

CNV leakage can be graded by fluorescein angiography, and in the clinical settting CNV leakage seems to correlate with CNV activity. AIF-deficient mice showed a trend toward a greater number of large, leaky, grade-2B lesions (denoting clinical significant leakage) than WT mice 2 weeks after laser (Figure 4).

AIF Deficiency Promotes Expansion of the Corneal Neovascularization and Retards Regression

Laser injury-induced choroidal neovascularization captures many of the important features of human conditions (ie, age-related macular degeneration), although this model includes various biological responses, such as thermal burn, tissue destruction, apoptosis and necrosis of retinal pigment epithelial cells, choroidal melanocytes, photoreceptors, or disruption of Bruch's membrane, and so forth. To clarify the role of AIF in VEGF-A–dependent angiogenesis, we used a simpler corneal pocket assay to induce angiogenesis in the corneas with AIF-deficient mice and WT mice. VEGF-A was implanted into these mice and the time course of VEGF-A–induced angiogenesis was followed until day 140. On day 6 after VEGF-A stimulation, the angiogenic

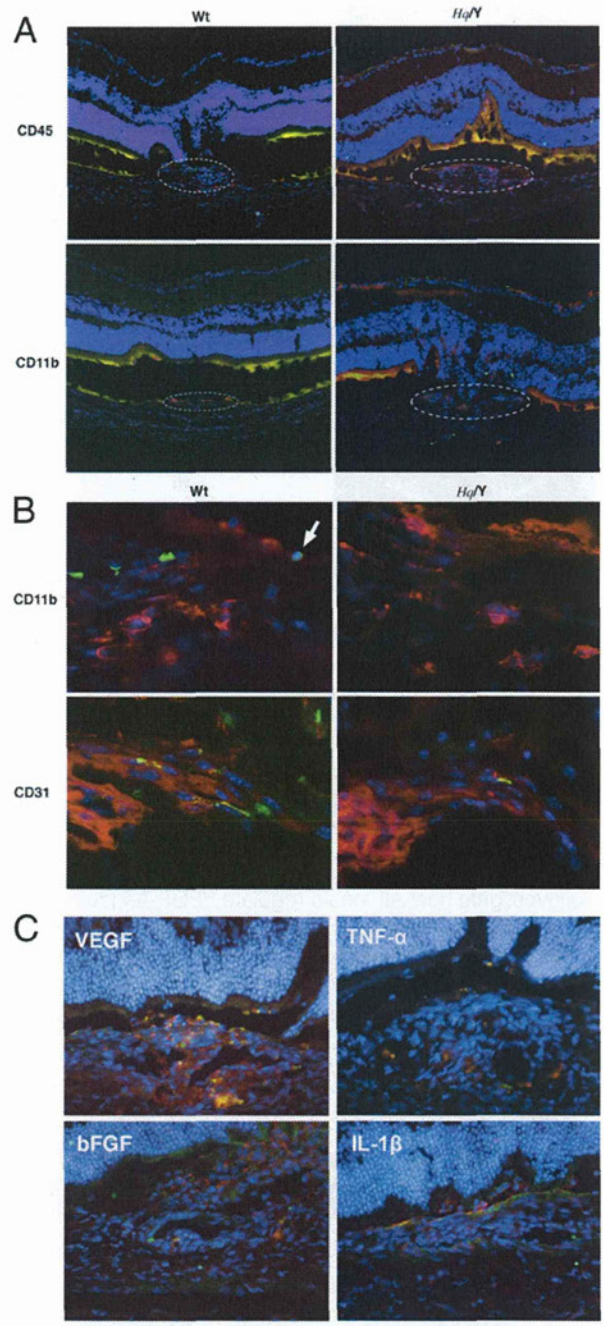

Figure 3. Immunohistochemistry for inflammatory and endothelial cells in CNV, which is observed at the laser injury site. A larger number of myeloid lineage cells (CD45) and macrophages (CD11b) migrate into CNV in apoptosis-inducing factor (AIF)-deficient mice compared to WT mice (**A**). $TUNEL^+$ inflammatory and endothelial cells are abundant in WT mice compared to AIF-deficient mice (**A**, **B**). **C:** Immunohistochemistry of CD11b and four major angiogenic or inflammatory factors (VEGF, TNF-α, bFGF, and IL-1β) were examined in the CNV. These four factors are expressed in CD11b-positive macrophages. VEGF is strongly expressed in neovascular tissue; however, it is especially expressed in the macrophages. AIF-deficiency enhances macrophage accumulation and angiogenic factor expression in the CNV. bFGF, basic fibroblast growth factor; Hq/Y, harlequin hemizygous male mice.

area in AIF-deficient mice was similar with WT mice, but by day 10 AIF-deficient mice showed a significantly greater area of corneal neovascularization than WT mice (Figure 5). The peak of the corneal neovascularization shifted from day

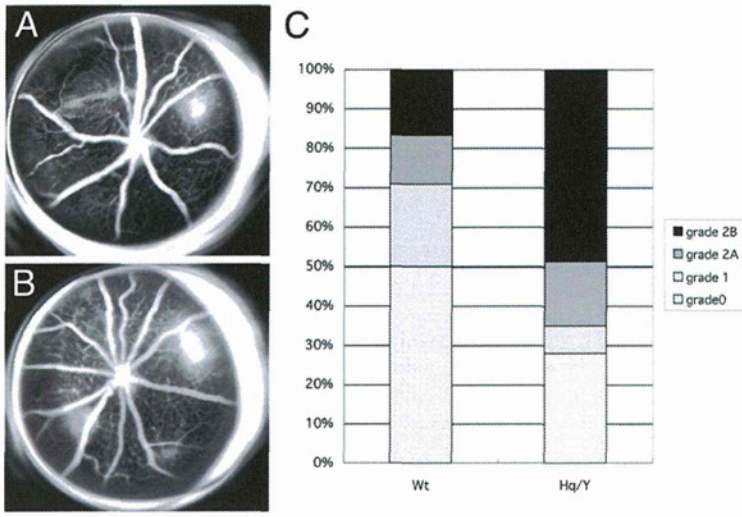

Figure 4. Fluorescein angiography of the laser-induced CNV. Compared to WT mice (**A**), AIF-deficient mice (**B**) developed larger CNV formation and more severe leakage. **C:** Lesions were graded on an ordinal scale based on the spatial and temporal evolution of fluorescein leakage as follows: grade 0 (nonleaky): no leakage, faint hyperfluorescence, or mottled fluorescence without leakage; grade 1 (questionable leakage): hyperfluorescent lesion without progressive increase in size or intensity; grade 2A (leaky): hyperfluorescence increasing in intensity but not in size; no definite leakage; grade 2B (pathologically significant leakage): hyperfluorescence increasing in intensity and in size; definite leakage. Hq/Y, harlequin hemizygous male mice.

28 in WT mice to day 56 in AIF-deficient mice. These data suggest that AIF may regulate VEGF-A-dependent angiogenesis at later stages of the process rather than the earlier step of angiogenic sprouting.

AIF Deficiency Decreases Apoptosis of Infiltrating Macrophages and Neovascular Endothelial Cells in VEGF-A-Induced Corneal Neovascularization

To investigate how AIF could regulate VEGF-A-induced angiogenesis, we hypothesized that cellular apoptosis by AIF could regulate the angiogenesis and checked apoptotic cells in VEGF-A-implanted AIF-deficient and WT mice with TUNEL staining. Immunostaining showed abundant infiltrated inflammatory cells (CD11b) and migrated neovascular endothelial cells (CD31) in AIF-deficient mice compared to WT mice (Figure 6A). Less TUNEL$^+$ cells in AIF-deficient mice could be observed than in WT mice at day 6 and at day 14 after VEGF-A implantation (Figure 6B). More TUNEL$^+$ apoptotic cells are noted on day 6 (early) than on day 14 (late) in WT mice. In contrast, more apoptotic cells are observed on day 14 (late) in AIF-deficient mice. AIF deficiency retarded cellular apoptosis in corneal neovascularization. These data suggest AIF could be important for cellular apoptosis during VEGF-A-induced angiogenesis.

Peritoneal Macrophages Are Resistant to Apoptosis in AIF-Deficient Mice

AIF deficiency promoted choroidal and corneal neovascularization, as well as accumulation of inflammatory cells (ie, CD45, 11b positive cells) at the local sites. To

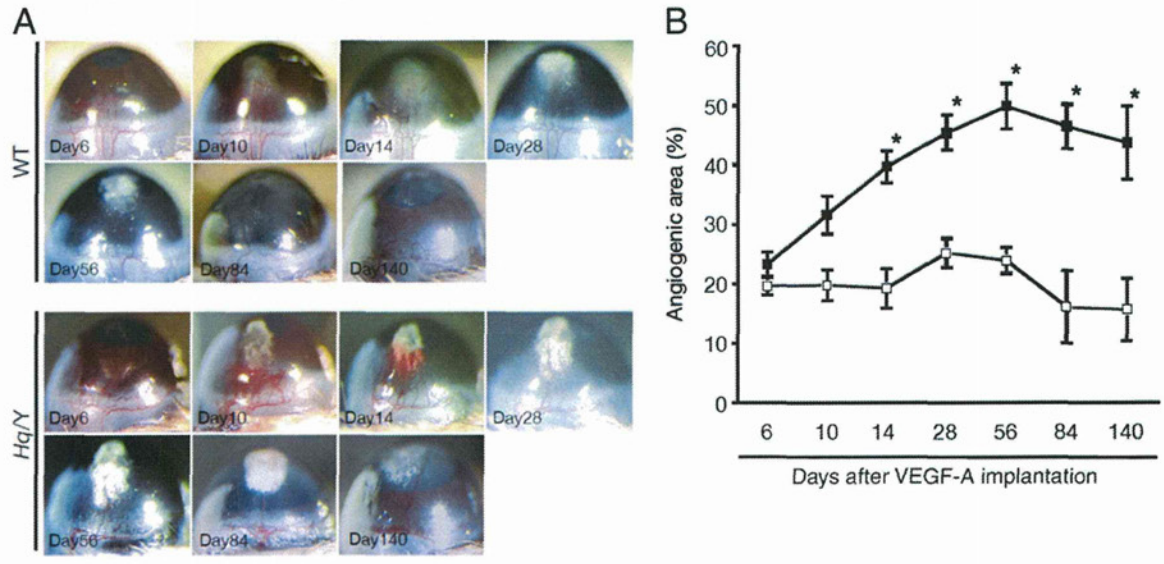

Figure 5. A: VEGF-induced corneal neovascularization by corneal micropocket assay. **B:** Pellets were implanted in the cornea, and the quantitative analysis of neovascularization in the mouse corneas was performed using image software. AIF-deficient mice (black box) develop larger neovascularization than WT mice (white box). The regression of the formed neovascularization is retarded in AIF-deficient mice compared to WT mice (**A**, **B**). Hq/Y, harlequin hemizygous male mice.

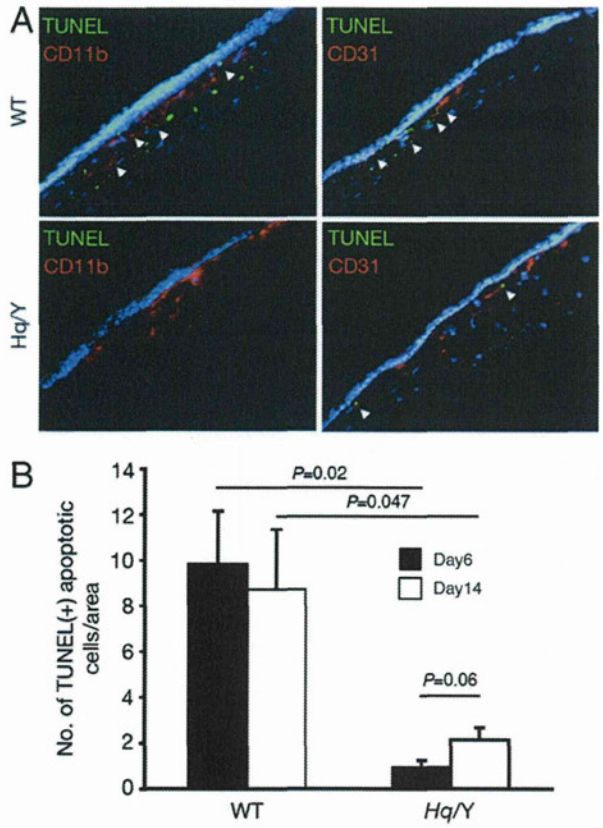

Figure 6. Immunohistochemistry for inflammatory and endothelial cells in the corneal micropocket assay. **A:** Immunostaining shows abundant infiltrated inflammatory cells (CD11b) and migrated neovascular endothelial cells (CD31) in AIF-deficient mice compared to WT mice. **B:** More TUNEL$^+$ apoptotic cells are observed in WT mice than in AIF-deficient mice. TUNEL$^+$ apoptotic cells had a trend to decrease on day 14 (late) in WT mice. In contrast, apoptotic cells had a trend to increase on day 14 (late) in AIF-deficient mice. Hq/Y, harlequin hemizygous male mice.

test the hypothesis that macrophages from AIF-deficient mice are resistant to apoptotic stimuli, we examined primary macrophage culture from Hq and WT mice. Peritoneal macrophages were collected and cultured with or without starvation. TUNEL$^+$ apoptotic macrophage increased after starvation, and AIF translocation from the cytosol into the nuclei were noted in these cells undergoing apoptosis (Figure 7). AIF deficiency diminished AIF translocation and protected macrophages from apoptotic cell death.

Discussion

AIF deficiency substantially expanded and prolonged formation of neovascularization, and retarded regression of neovascularization in both laser injury CNV- and VEGF-induced corneal neovascularization models. Furthermore, both anatomical and functional metrics of CNV (flat mount analysis and fluorescein angiography) supported the notion that AIF deficiency leads to more robust and larger neovascularization. We have reported that laser photocoagulation incites inflammation, leading to endothelial upregulation of intercellular adhesion molecule-1, which binds to CD18, mediating firm leukocyte-endothelial adhesion and transmigration.[34] Laser photocoagulation leads to production of VEGF by retinal pigment epithelial cells,[20,39] stimulating proliferation of adjacent choroidal vascular endothelium and upregulation of intercellular adhesion molecule-1 expression on endothelium.[40] Circulating leukocytes, which migrate in response to VEGF, also release VEGF, amplifying the locally produced VEGF response as they bind to the endothelium. In addition, leukocyte-derived cytokines can stimulate retinal pigment epithelial cells and fibroblasts to express VEGF,[41,42] as well as the chemotaxins IL-8, monocyte chemotactic protein-1,[43] metalloproteinases[44] and intercellular adhesion molecule-1.[45] These observations are consistent with our findings that AIF deficiency protected macrophages and neovascular endothelial cells from apoptosis, result in accumulation and prolongation of inflammatory macrophages and neovascular endothelial cells at the site of the developing neovascularization.

Macrophages have been shown to exhibit distinct functions during injury and repair, especially in neovascularization. We have reported that macrophages are

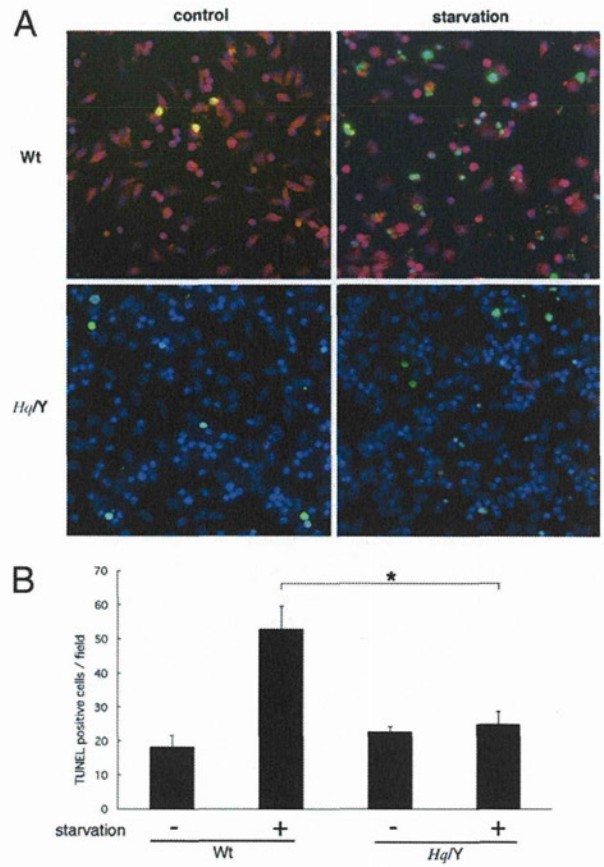

Figure 7. Peritoneal macrophage culture under starvation. Macrophages were collected from the peritoneal space and cultured using serum-free medium. **A:** WT mice show cytosolic (normal) and nuclear (apoptotic) staining for AIF, whereas AIF-deficient mice show no staining. **B:** TUNEL$^+$ apoptotic macrophages increase after 24 hours of starvation in WT mice. In contrast, macrophages from AIF-deficient mice are resistant to starvation. $^*P < 0.05$. Hq/Y, harlequin hemizygous male mice.

localized to the site of tissue injury before the onset of neovascularization and systemic macrophage depletion resulted in reduced pathological neovascularization in CNV,[21] and corneal neovascularization.[42] In clinical settings of age-related macular degeneration, it is known that chronic inflammatory responses caused by accumulation of lipids and/or immune complex induce further infiltration of inflammatory cells, and CNV.[46] In the current study, cultured peritoneal macrophages from AIF-deficient mice are resistant to apoptotic stimuli, compared to macrophages from WT mice. In line with these *in vitro* observations, immunohistochemistry showed accumulation and prolongation of macrophages at the site in both laser-induced CNV and VEGF-induced corneal neovascularization *in vivo* in AIF-deficient mice. Thus, AIF deficiency decreased effective apoptotic clearance of excessive inflammatory cells that induced robust and larger neovascularization.

Pathological angiogenesis is controlled by the balance of proangiogenic factors and anti-angiogenic factors. Several proapoptotic molecules have been identified among anti-angiogenic factors that help regulate angiogenesis, including Fas-ligand, thrombospondin-1, and endostatin. The concept that the balance between pro- and anti-apoptotic factors plays a critical role in the regulation of angiogenesis has been postulated for ocular neovascularization.[47–49] The reports, however, mainly focus on the death receptor family (ie, Fas/Fas-Ligand) and subsequent caspase signaling.[48,50–52] Cell death in vertebrates, however, usually proceeds via the mitochondrial pathway of apoptosis.[1] In the current article, we focused on the phylogenetically old, death receptor-independent, caspase-independent proapoptotic factor, AIF that mainly signals mitochondrial pathway of apoptosis in mammalian cells.[7] We took advantage of AIF-deficient mice (*Hq*), which cause an 80% reduction of functional proapoptotic protein, AIF.[14] Blockade of mitochondrial pathway of apoptosis by AIF substantially accumulated and prolonged inflammatory macrophages and neovascular endothelial cells, resulting in expanding and prolonging destructive inflammation and leakage at the site. Furthermore, recent data has revealed that AIF modulate active caspase-independent necrotic pathways defined as necroptosis (programmed necrosis) additionally to apoptosis.[53] AIF and the key executioner, such as the kinase, the receptor-interacting protein 1 have become potential therapeutic targets in apoptosis/necrosis.[14,54] In the current article, we hypothesized that decreased apoptotic cell death of inflammatory/endothelial cells may modulate CNV. The bone marrow transplantation experiments also support the hypothesis that reconstructed WT macrophages partially reversed CNV modulation in AIF-deficient mice. Further study is needed to clarify the direct molecular mechanism underlying the phenomena.

Therapeutic strategies directed against pathological neovascularization via appropriate apoptotic clearance of excessive inflammatory cells or endothelial cells may have potential as a novel clinically relevant approach in addition to conventional therapies.

Acknowledgments

We thank Mari Imamura and Fumiyo Morikawa (Kyushu University) and Kennard Thomas, Sreedevi Mallemadugula, Norman Michaud, and Miin Roh (Massachusetts Eye and Ear Infirmary) for their technical assistance. We also thank the Massachusetts Lions Research Fund for generous funds provided for laboratory equipment used in this project and Research to Prevent Blindness for unrestricted funds awarded to the Department of Ophthalmology at Harvard Medical School.

References

1. Green DR, Kroemer G: The pathophysiology of mitochondrial cell death. Science 2004, 305:626–629
2. Bao Q, Riedl SJ, Shi Y: Structure of Apaf-1 in the auto-inhibited form: a critical role for ADP. Cell Cycle 2005, 4:1001–1003
3. Bao Q, Shi Y: Apoptosome: a platform for the activation of initiator caspases. Cell Death Differ 2007, 14:56–65
4. Acehan D, Jiang X, Morgan DG, Heuser JE, Wang X, Akey CW: Three-dimensional structure of the apoptosome: implications for assembly, procaspase-9 binding, and activation. Mol Cell 2002, 9:423–432
5. Bouchier-Hayes L, Lartigue L, Newmeyer DD: Mitochondria: pharmacological manipulation of cell death. J Clin Invest 2005, 115:2640–2647
6. Hisatomi T, Sakamoto T, Murata T, Yamanaka I, Oshima Y, Hata Y, Ishibashi T, Inomata H, Susin SA, Kroemer G: Relocalization of apoptosis-inducing factor in photoreceptor apoptosis induced by retinal detachment in vivo. Am J Pathol 2001, 158:1271–1278
7. Susin SA, Lorenzo HK, Zamzami N, Marzo I, Snow BE, Brothers GM, Mangion J, Jacotot E, Costantini P, Loeffler M: Molecular characterization of mitochondrial apoptosis-inducing factor. Nature 1999, 397:441–446
8. Kroemer G, Martin SJ: Caspase-independent cell death. Nat Med 2005, 11:725–730
9. Hisatomi T, Ishibashi T, Miller JW, Kroemer G: Pharmacological inhibition of mitochondrial membrane permeabilization for neuroprotection. Exp Neurol 2009, 218:347–352
10. Cande C, Vahsen N, Kouranti I, Schmitt E, Daugas E, Spahr C, Luban J, Kroemer RT, Giordanetto F, Garrido C: AIF and cyclophilin A cooperate in apoptosis-associated chromatinolysis. Oncogene 2004, 23:1514–1521
11. Joza N, Oudit GY, Brown D, Benit P, Kassiri Z, Vahsen N, Benoit L, Patel MM, Nowikovsky K, Vassault A: Muscle-specific loss of apoptosis-inducing factor leads to mitochondrial dysfunction, skeletal muscle atrophy, and dilated cardiomyopathy. Mol Cell Biol 2005, 25:10261–10272
12. Hisatomi T, Sakamoto T, Goto Y, Yamanaka I, Oshima Y, Hata Y, Ishibashi T, Inomata H, Susin SA, Kroemer G: Critical role of photoreceptor apoptosis in functional damage after retinal detachment. Curr Eye Res 2002, 24:161–172
13. Hisatomi T, Sakamoto T, Sonoda KH, Tsutsumi C, Qiao H, Enaida H, Yamanaka I, Kubota T, Ishibashi T, Kura S: Clearance of apoptotic photoreceptors: elimination of apoptotic debris into the subretinal space and macrophage-mediated phagocytosis via phosphatidylserine receptor and integrin alphavbeta3. Am J Pathol 2003, 162:1869–1879
14. Hisatomi T, Nakazawa T, Noda K, Almulki L, Miyahara S, Nakao S, Ito Y, She H, Kohno R, Michaud N: HIV protease inhibitors provide neuroprotection through inhibition of mitochondrial apoptosis in mice. J Clin Invest 2008, 118:2025–2038
15. Murakami Y, Ikeda Y, Yonemitsu Y, Onimaru M, Nakagawa K, Kohno R, Miyazaki M, Hisatomi T, Nakamura M, Yabe T: Inhibition of nuclear translocation of apoptosis-inducing factor is an essential mechanism of the neuroprotective activity of pigment epithelium-derived factor in a rat model of retinal degeneration. Am J Pathol 2008, 173:1326–1338
16. Notomi S, Hisatomi T, Kanemaru T, Takeda A, Ikeda Y, Enaida H, Kroemer G, Ishibashi T: Critical involvement of extracellular ATP

acting on P2RX7 purinergic receptors in photoreceptor cell death. Am J Pathol 2011, 179:2798–2809
17. Wang H, Shimoji M, Yu SW, Dawson TM, Dawson VL: Apoptosis inducing factor and PARP-mediated injury in the MPTP mouse model of Parkinson's disease. Ann NY Acad Sci 2003, 991:132–139
18. Chu CT, Zhu JH, Cao G, Signore A, Wang S, Chen J: Apoptosis inducing factor mediates caspase-independent 1-methyl-4-phenylpyridinium toxicity in dopaminergic cells. J Neurochem 2005, 94: 1685–1695
19. Sanges D, Comitato A, Tammaro R, Marigo V: Apoptosis in retinal degeneration involves cross-talk between apoptosis-inducing factor (AIF) and caspase-12 and is blocked by calpain inhibitors. Proc Natl Acad Sci USA 2006, 103:17366–17371
20. Ishibashi T, Hata Y, Yoshikawa H, Nakagawa K, Sueishi K, Inomata H: Expression of vascular endothelial growth factor in experimental choroidal neovascularization. Graefes Arch Clin Exp Ophthalmol 1997, 235:159–167
21. Tsutsumi C, Sonoda KH, Egashira K, Qiao H, Hisatomi T, Nakao S, Ishibashi M, Charo IF, Sakamoto T, Murata T: The critical role of ocular-infiltrating macrophages in the development of choroidal neovascularization. J Leukoc Biol 2003, 74:25–32
22. Gaengel K, Genove G, Armulik A, Betsholtz C: Endothelial-mural cell signaling in vascular development and angiogenesis. Arterioscler Thromb Vasc Biol 2009, 29:630–638
23. Patan S: TIE1 and TIE2 receptor tyrosine kinases inversely regulate embryonic angiogenesis by the mechanism of intussusceptive microvascular growth. Microvasc Res 1998, 56:1–21
24. Jones N, Voskas D, Master Z, Sarao R, Jones J, Dumont DJ: Rescue of the early vascular defects in Tek/Tie2 null mice reveals an essential survival function. EMBO Rep 2001, 2:438–445
25. Dimmeler S, Zeiher AM: Endothelial cell apoptosis in angiogenesis and vessel regression. Circ Res 2000, 87:434–439
26. Miller JW, Walsh AW, Kramer M, Hasan T, Michaud N, Flotte TJ, Haimovici R, Gragoudas ES: Photodynamic therapy of experimental choroidal neovascularization using lipoprotein-delivered benzoporphyrin. Arch Ophthalmol 1995, 113:810–818
27. Zacks DN, Ezra E, Terada Y, Michaud N, Connolly E, Gragoudas ES, Miller JW: Verteporfin photodynamic therapy in the rat model of choroidal neovascularization: angiographic and histologic characterization. Invest Ophthalmol Vis Sci 2002, 43:2384–2391
28. Hisatomi T, Sakamoto T, Yamanaka I, Sassa Y, Kubota T, Ueno H, Ohnishi Y, Ishibashi T: Photocoagulation-induced retinal gliosis is inhibited by systemically expressed soluble TGF-beta receptor type II via adenovirus mediated gene transfer. Lab Invest 2002, 82:863–870
29. She H, Nakazawa T, Matsubara A, Hisatomi T, Young TA, Michaud N, Connolly E, Hafezi-Moghadam A, Gragoudas ES, Miller JW: Reduced photoreceptor damage after photodynamic therapy through blockade of nitric oxide synthase in a model of choroidal neovascularization. Invest Ophthalmol Vis Sci 2007, 48:2268–2277
30. She H, Nakazawa T, Matsubara A, Connolly E, Hisatomi T, Noda K, Kim I, Gragoudas ES, Miller JW: Photoreceptor protection after photodynamic therapy using dexamethasone in a rat model of choroidal neovascularization. Invest Ophthalmol Vis Sci 2008, 49:5008–5014
31. Noda K, She H, Nakazawa T, Hisatomi T, Nakao S, Almulki L, Zandi S, Miyahara S, Ito Y, Thomas KL: Vascular adhesion protein-1 blockade suppresses choroidal neovascularization. FASEB J 2008, 22: 2928–2935
32. Westerhof GR, Ploemacher RE, Boudewijn A, Blokland I, Dillingh JH, McGown AT, Hadfield JA, Dawson MJ, Down JD: Comparison of different busulfan analogues for depletion of hematopoietic stem cells and promotion of donor-type chimerism in murine bone marrow transplant recipients. Cancer Res 2000, 60:5470–5478
33. Hisatomi T, Sonoda KH, Ishikawa F, Qiao H, Nakazawa T, Fukata M, Nakamura T, Noda K, Miyahara S, Harada M: Identification of resident and inflammatory bone marrow derived cells in the sclera by bone marrow and haematopoietic stem cell transplantation. Br J Ophthalmol 2007, 91:520–526
34. Sakurai E, Taguchi H, Anand A, Ambati BK, Gragoudas ES, Miller JW, Adamis AP, Ambati J: Targeted disruption of the CD18 or ICAM-1 gene inhibits choroidal neovascularization. Invest Ophthalmol Vis Sci 2003, 44:2743–2749
35. Maruyama K, Ii M, Cursiefen C, Jackson DG, Keino H, Tomita M, Van Rooijen N, Takenaka H, D'Amore PA, Stein-Streilein J: Inflammation-induced lymphangiogenesis in the cornea arises from CD11b-positive macrophages. J Clin Invest 2005, 115:2363–2372
36. Nakazawa T, Hisatomi T, Nakazawa C, Noda K, Maruyama K, She H, Matsubara A, Miyahara S, Nakao S, Yin Y: Monocyte chemoattractant protein 1 mediates retinal detachment-induced photoreceptor apoptosis. Proc Natl Acad Sci USA 2007, 104:2425–2430
37. Barber BR: Research news. Mouse News Lett 1971, 45:34–35
38. Klein JA, Longo-Guess CM, Rossmann MP, Seburn KL, Hurd RE, Frankel WN, Bronson RT, Ackerman SL: The harlequin mouse mutation downregulates apoptosis-inducing factor. Nature 2002, 419:367–374
39. Wada M, Ogata N, Otsuji T, Uyama M: Expression of vascular endothelial growth factor and its receptor (KDR/flk-1) mRNA in experimental choroidal neovascularization. Curr Eye Res 1999, 18:203–213
40. Miyamoto K, Khosrof S, Bursell SE, Moromizato Y, Aiello LP, Ogura Y, Adamis AP: Vascular endothelial growth factor (VEGF)-induced retinal vascular permeability is mediated by intercellular adhesion molecule-1 (ICAM-1). Am J Pathol 2000, 156:1733–1739
41. Oh H, Takagi H, Takagi C, Suzuma K, Otani A, Ishida K, Matsumura M, Ogura Y, Honda Y: The potential angiogenic role of macrophages in the formation of choroidal neovascular membranes. Invest Ophthalmol Vis Sci 1999, 40:1891–1898
42. Nakao S, Kuwano T, Tsutsumi-Miyahara C, Ueda S, Kimura YN, Hamano S, Sonoda KH, Saijo Y, Nukiwa T, Strieter RM: Infiltration of COX-2-expressing macrophages is a prerequisite for IL-1 beta-induced neovascularization and tumor growth. J Clin Invest 2005, 115:2979–2991
43. Holtkamp GM, Van Rossem M, de Vos AF, Willekens B, Peek R, Kijlstra A: Polarized secretion of IL-6 and IL-8 by human retinal pigment epithelial cells. Clin Exp Immunol 1998, 112:34–43
44. Peppin GJ, Weiss SJ: Activation of the endogenous metalloproteinase, gelatinase, by triggered human neutrophils. Proc Natl Acad Sci USA 1986, 83:4322–4326
45. Elner SG, Elner VM, Pavilack MA, Todd RF, 3rd, Mayo-Bond L, Franklin WA, Strieter RM, Kunkel SL, Huber AR: Modulation and function of intercellular adhesion molecule-1 (CD54) on human retinal pigment epithelial cells. Lab Invest 1992, 66:200–211
46. Ishibashi T, Patterson R, Ohnishi Y, Inomata H, Ryan SJ: Formation of drusen in the human eye. Am J Ophthalmol 1986, 101:342–353
47. Wang S, Sorenson CM, Sheibani N: Attenuation of retinal vascular development and neovascularization during oxygen-induced ischemic retinopathy in Bcl-2−/− mice. Dev Biol 2005, 279:205–219
48. Davies MH, Eubanks JP, Powers MR: Increased retinal neovascularization in Fas ligand-deficient mice. Invest Ophthalmol Vis Sci 2003, 44:3202–3210
49. Davies MH, Stempel AJ, Powers MR: MCP-1 deficiency delays regression of pathologic retinal neovascularization in a model of ischemic retinopathy. Invest Ophthalmol Vis Sci 2008, 49:4195–4202
50. Ilg RC, Davies MH, Powers MR: Altered retinal neovascularization in TNF receptor-deficient mice. Curr Eye Res 2005, 30:1003–1013
51. Semkova I, Fauser S, Lappas A, Smyth N, Kociok N, Kirchhof B, Paulsson M, Poulaki V, Joussen AM: Overexpression of FasL in retinal pigment epithelial cells reduces choroidal neovascularization. FASEB J 2006, 20:1689–1691
52. Hubert KE, Davies MH, Stempel AJ, Griffith TS, Powers MR: TRAIL-deficient mice exhibit delayed regression of retinal neovascularization. Am J Pathol 2009, 175:2697–2708
53. Delavallee L, Cabon L, Galan-Malo P, Lorenzo HK, Susin SA: AIF-mediated caspase-independent necroptosis: a new chance for targeted therapeutics. IUBMB Life 63:221–232
54. Trichonas G, Murakami Y, Thanos A, Morizane Y, Kayama M, Debouck CM, Hisatomi T, Miller JW, Vavvas DG: Receptor interacting protein kinases mediate retinal detachment-induced photoreceptor necrosis and compensate for inhibition of apoptosis. Proc Natl Acad Sci USA 2010, 107:21695–21700

Hindawi Publishing Corporation
Evidence-Based Complementary and Alternative Medicine
Volume 2012, Article ID 513638, 8 pages
doi:10.1155/2012/513638

Review Article

Evaluation of the Effects of Acupuncture on Blood Flow in Humans with Ultrasound Color Doppler Imaging

Shin Takayama,[1] Masashi Watanabe,[1] Hiroko Kusuyama,[1] Satoru Nagase,[2] Takashi Seki,[1] Toru Nakazawa,[3] and Nobuo Yaegashi[1,2]

[1] *Department of Traditional Asian Medicine, Graduate School of Medicine, Tohoku University, 2-1, Seiryo-machi, Aoba-ku, Sendai 980-8575, Japan*
[2] *Department of Obstetrics and Gynecology, Tohoku University Graduate School of Medicine, Sendai 980-8574, Japan*
[3] *Department of Ophthalmology and Visual Science, Graduate School of Medicine, Tohoku University, Sendai 980-8575, Japan*

Correspondence should be addressed to Shin Takayama, tatahara1492@gmail.com

Received 23 February 2012; Revised 2 April 2012; Accepted 2 April 2012

Academic Editor: Gerhard Litscher

Color Doppler imaging (CDI) can be used to noninvasively create images of human blood vessels and quantitatively evaluate blood flow in real-time. The purpose of this study was to assess the effects of acupuncture on the blood flow of the peripheral, mesenteric, and retrobulbar arteries by CDI. Statistical significance was defined as P values less than 0.05. Blood flow in the radial and brachial arteries was significantly lower during needle stimulation on LR3 than before in healthy volunteers, but was significantly higher after needle stimulation than before. LR3 stimulation also resulted in a significant decrease in the vascular resistance of the short posterior ciliary artery and no significant change of blood flow through the superior mesenteric artery (SMA) during acupuncture. In contrast, ST36 stimulation resulted in a significant increase in blood flow through the SMA and no significant change in the vascular resistance of the retrobulbar arteries. Additionally, acupuncture at previously determined acupoints in patients with open-angle glaucoma led to a significant reduction in the vascular resistance of the central retinal artery and short posterior ciliary artery. Our results suggest that acupuncture can affect blood flow of the peripheral, mesenteric, and retrobulbar arteries, and CDI can be useful to evaluate hemodynamic changes by acupuncture.

1. Introduction

To date, no quantitative evaluation methods have been established for determining the physiological effectiveness of acupuncture. Therefore, researchers conduct experiments using a variety of approaches. In this study, we focused on the physiological reactions to acupuncture and investigated blood flow changes that result from acupuncture [1–5].

Many studies of acupuncture efficacy have been based on the results of animal experiments with anesthesia. These studies indicate that acupuncture works through physiological mechanisms that occur primarily in the autonomic nervous system [6–12]. When acupuncture is performed in human clinical practice, the conditions are very different from those in animal experiments. Additionally, because the invasive examination techniques that are often used to evaluate the results of acupuncture treatments affect the efficacy of those treatments, it is difficult to distinguish physiological reactions caused by acupuncture from those caused by the invasion necessary for examination. To determine the efficacy of acupuncture in humans, it is important that the examination method be noninvasive. We therefore used noninvasive color Doppler imaging (CDI) with ultrasound to evaluate blood flow. CDI is an examination technique that is widely used in the practice and research of Western medicine [13–21]. CDI can quantitatively measure intravascular blood flow in the extremities and in various organs in real-time. It is useful in the investigation of vessels, such as the peripheral, coronary, splenic, adrenal, and superior mesenteric arteries (SMA) [22]. In addition, the reproducibility of real-time and noninvasive hemodynamic measurement with CDI is reported elsewhere [23].

In traditional Chinese medicine, LR3 (Taichong, located on the foot, 1.5–2 units above the web between the

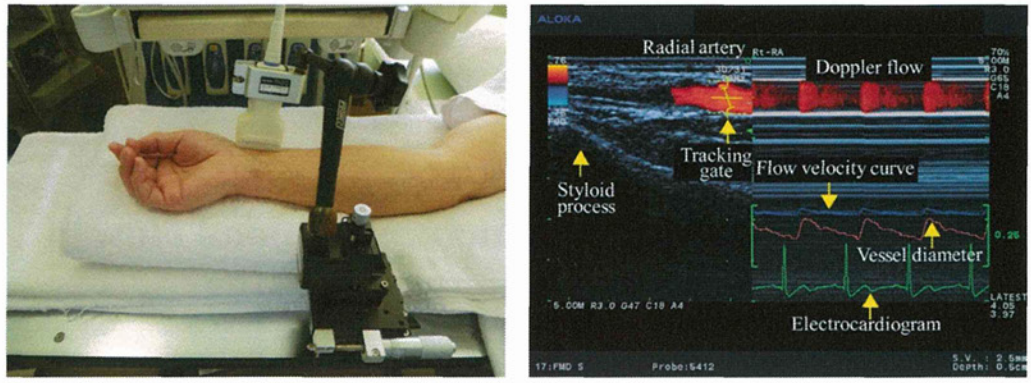

(a) (b)

FIGURE 1: (a) Ultrasound measurement of the radial artery. 13 MHz linear transducer is fixed along radial artery with a special probe holder (MP-PH0001, Aloka Co., Ltd., Tokyo, Japan). (b) Display of CDI. Left: the vessel image and the position of the artery tracking gate. Right: changes in vessel diameter, Doppler flow, and flow velocity as determined by an automated edge-detection device and computer analysis software (e-Tracking system; Aloka Co., Ltd., Tokyo, Japan).

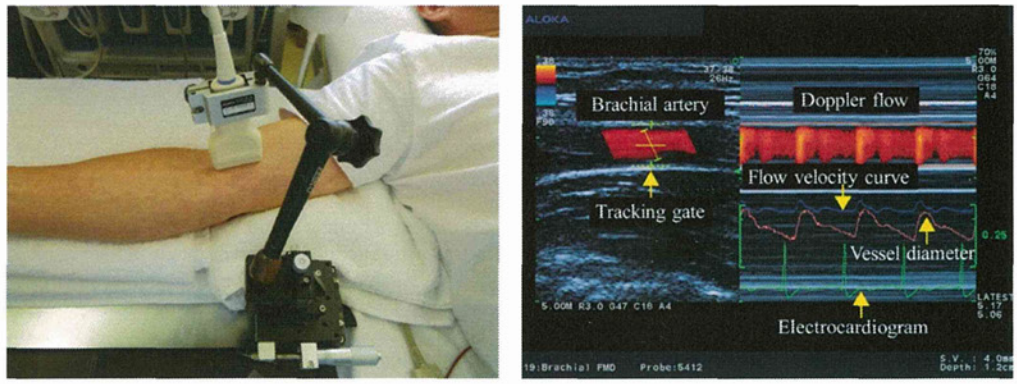

(a) (b)

FIGURE 2: (a) Ultrasound measurement of the brachial artery. 13 MHz linear transducer is fixed along brachial artery with a special probe holder (MP-PH0001, Aloka Co., Ltd., Tokyo, Japan). (b) Display of CDI. Left: image of the vessel image and position of the artery tracking gate. Right: changes in vessel diameter, Doppler flow, and flow velocity, as determined by an automated edge detection device and computer analysis software (e-Tracking system; Aloka Co., Ltd., Tokyo, Japan).

first and second toes [24]) is an acupoint on the liver meridian, which has the functions of "soothing the liver," "regulating the blood," and "opening into the eyes" [24]. We therefore hypothesized that LR3 acupuncture would affect hemodynamics in the peripheral arteries and the retrobulbar arteries. ST36 (Zusanli, located on the lower leg, 3 units below the lateral "eye" of the knee, approximately 1 finger width lateral to the tibia [24]), in contrast, is an acupoint on the stomach meridian, and is associated with the functions of gastrointestinal organs [25]. We therefore hypothesized that ST36 acupuncture would affect hemodynamics in the SMA. Because glaucoma prognosis and retrobulbar circulation are related [26–29], we also investigated the effects of acupuncture on retrobulbar circulation in open-angle glaucoma (OAG) patients. In this study, we introduce the noninvasive CDI with ultrasound to evaluate blood flow changes by acupuncture.

2. Materials and Methods

2.1. Ultrasound Technique for Blood Flow Measurement. We measured circulation in the upper limb, SMA, and retrobulbar vessels using an ultrasound system (Prosound α10; Aloka Co., Ltd, Tokyo, Japan). The system had a 13 MHz linear transducer and a 5 MHz convex transducer. We used the linear transducer to examine peripheral arteries and the retrobulbar vessels. We used the convex transducer to measure SMA circulation.

The radial artery was examined just medial to the radial styloid process (Figure 1). The brachial artery was monitored immediately proximal to the elbow (Figure 2). The SMA supplies blood to the whole small intestine, except for the superior part of the duodenum. It also supplies blood to the cecum, the ascending colon, and most of the transverse colon. SMA measurements were acquired within 2-3 cm of

(a) (b)

FIGURE 3: (a) Ultrasound measurement of the SMA. 5 MHz convex transducer is positioned on the abdomen. (b) Display of CDI. Left: image of the vessel and the position of the artery tracking. Right: Doppler flow and flow velocity.

the artery origin (Figure 3) [30, 31]. Avoiding any pressure on the eye, CDI was performed for the retrobulbar vessels, including the ophthalmic artery (OA), central retinal artery (CRA), and nasal or temporal short posterior ciliary artery (Figures 4 and 5). The OA was examined approximately 20 mm behind the globe (Figure 5(b)), the CRA was examined within 5 mm of the retrolaminar portion of the optic nerve (Figure 5(c)), and the nasal or temporal SPCA that obtained clear image was examined approximately 5–10 mm behind the globe (Figure 5(d)). Blood flow was monitored continuously [32, 33] and we employed a Doppler angle of 60° or less for each measurement [34, 35]. Each Doppler waveform was automatically drawn and calculated using the software included with the ultrasound system. The following calculations were used to determine the hemodynamic parameters at each site [30, 31].

(i) Vessel diameter (VD).

(ii) Cross-sectional area (CSA) = $(\mathrm{VD}/2)^2 \times \pi$.

(iii) Peak systolic velocity (PSV).

(iv) End-diastolic velocity (EDV).

(v) Resistive index (RI) = (PSV − EDV)/PSV.

(vi) Mean flow velocity (MV).

(vii) Blood flow volume = CSA × MV.

2.2. Statistical Analysis. Statistical analysis was performed with SPSS software (version 16.0, SPSS Japan Inc., Tokyo, Japan). Repeated measure analysis of variance, followed by Dunnett's post hoc test, was used for statistical comparison between the measure points. Comparison between rest and after acupuncture was done by paired t-test. Results are presented as the mean ± SD and $P < 0.05$ was taken to indicate significance for all statistical analysis.

2.3. Experiment 1: Effects of LR3 Acupuncture on Upper Limb Circulation [1]. This study was employed to investigate the upper limb circulation after acupuncture at LR3 acupoints on foot. The participants were recruited by the poster recruitment in Tohoku University. Eighteen healthy volunteers (mean age: 32 ± 5 years; 14 males and 4 females) were enrolled in this study. A disposable fine stainless-steel needle (diameter: 0.16 mm; length: 40 mm; Seirin Co., Ltd., Shizuoka, Japan) was inserted on LR3 bilaterally and maintained at a depth of 10 mm during the test. After the needle was inserted, stimulation (rotating the needles manually within an angle of 90 degrees) was performed for 18 seconds. The needles were removed 200 seconds after acupuncture. Radial and brachial CDI were performed before acupuncture; during acupuncture treatment; 30, 60, and 180 seconds after acupuncture.

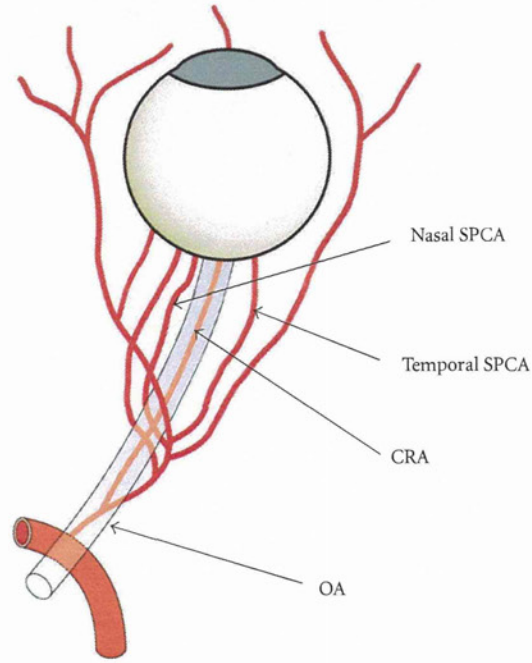

FIGURE 4: Schema of the retrobulbar arteries (OA: ophthalmic artery, CRA: central retinal artery, and SPCA: short posterior ciliary artery).

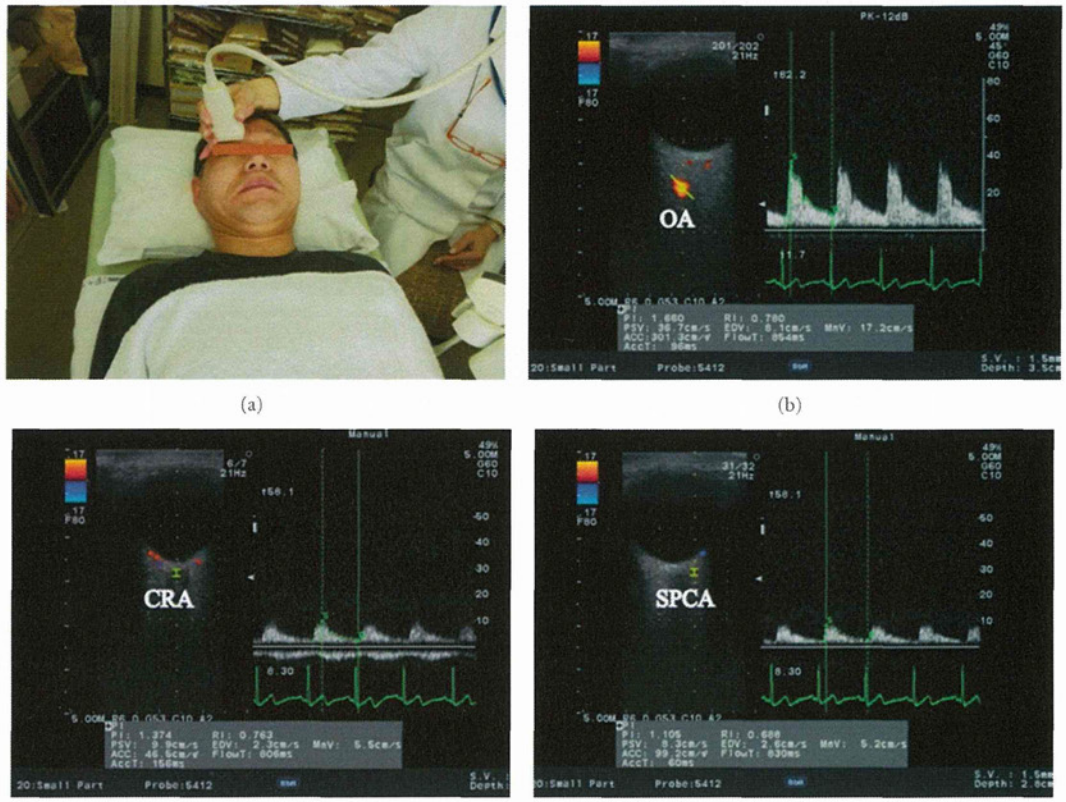

FIGURE 5: (a) Ultrasound measurement of retrobulbar arteries. 13 MHz linier transducer is attached on the eyelid. Horizontal scans by CDI through the ocular globe showing the (b) ophthalmic artery (OA), (c) central retinal artery (CRA), and (d) temporal short posterior ciliary artery (SPCA). Left: image of the vessel and the position of the artery tracking. Right: Doppler flow and flow velocity (b, c, and d).

2.4. Experiment 2: Effects of LR3 Acupuncture on Blood Circulation to the Eye and through the SMA. This study was employed to clarify the hemodynamic changes by acupuncture in two different organs (intestine and eye) with simultaneous evaluation by ultrasound. The participants were recruited by the poster recruitment in Tohoku University. Thirteen healthy volunteers (mean age: 36 ± 9 years; 10 males and 3 females) were enrolled in this study. Acupuncture was performed bilaterally on LR3 with manual needle rotation and the disposable stainless steel needles (0.16 mm × 40 mm; Seirin Co. Ltd., Shizuoka, Japan) were kept at the same site for 15 minutes. Retrobulbar vessels and SMA circulation were measured simultaneously at rest and 15 minutes after the start of acupuncture using ultrasound.

2.5. Experiment 3: Effects of ST36 Acupuncture Blood Circulation to the Eye and through the SMA. This study was also employed to clarify the hemodynamic changes by acupuncture in two different organs (intestine and eye) with simultaneous evaluation by ultrasound. The participants were recruited by the poster recruitment in Tohoku University. Thirteen subjects (mean age: 36 ± 8 years; 10 males and 3 females) were enrolled in this study. Acupuncture was performed bilaterally on ST36 with manual rotation of the disposable stainless steel needles (0.16 mm × 40 mm; Seirin Co. Ltd., Shizuoka, Japan) were kept in the same site for 15 minutes. Retrobulbar vessels and SMA circulation were measured simultaneously at rest and 15 minutes after the start of acupuncture using ultrasound.

2.6. Experiment 4: Effects of Acupuncture on Retrobulbar Circulation in OAG Patients [2]. The relation between glaucoma and retrobulbar circulation in the prognosis of the disease has been indicated [26–29], therefore we investigated the effects of acupuncture on OAG patients by CDI. The patients were recruited in the outpatient clinic of ophthalmology in Tohoku University Hospital. Eleven OAG patients (mean age: 63 ± 11 years; 1 male and 10 females; 20 eyes with OAG) were enrolled. All patients included in the study had been treated with topical antiglaucoma medications for at least 3 months prior to the study. As a control, the subjects received the measurements of retrobulbar vessel hemodynamics that were performed at rest and one hour after the first measurement. One month later, they received the same measurements before and after acupuncture treatment. Acupuncture was performed once bilaterally at acupoints BL2, EX-HN5, ST2, ST36, SP6, KI3, LR3, GB20, BL18, and BL23 for 15 minutes using disposable stainless steel needles

Table 1: Hemodynamic parameters and blood flow volume of the radial and brachial arteries by acupuncture on LR3. The values represent the mean and SD. $^{*}P < 0.05$, $^{**}P < 0.01$ versus before acupuncture. Modified from [1].

Parameters	Acupuncture on LR3				
	Before	During	30 s after	60 s after	180 s after
Systolic blood pressure (mmHg)	116.8 ± 10.1				114.5 ± 12.3
Diastolic blood pressure (mmHg)	67.3 ± 8.4				65.8 ± 7.3
Heart rate (beats/min)	67.3 ± 10.1	64.2 ± 8.8	65.8 ± 9.3	66.2 ± 9.3	66.9 ± 9.6
Blood flow volume of the radial artery (mL/min)	56.3 ± 33.5	25.4 ± 26.3	57.9 ± 47.5	67.7 ± 44.7	67.0 ± 36.5
Blood flow volume of the brachial artery (mL/min)	87.5 ± 56.4	65.7 ± 41.6	86.8 ± 53.7	90.1 ± 51.5	106.5 ± 59.8

Table 2: Hemodynamic parameters, blood flow volume of the SMA, and resistive index of retrobulbar arteries by acupuncture on LR3. The values represent the mean and SD. $^{*}P < 0.05$, $^{**}P < 0.01$ versus before acupuncture.

Parameters	Acupuncture on LR3	
	Before	After
Systolic blood pressure (mmHg)	119.6 ± 12.8	116.7 ± 11.1
Diastolic blood pressure (mmHg)	77.7 ± 9.4	76.5 ± 9.3
Heart rate (beats/min)	66.8 ± 7.1	63.3 ± 4.6**
Blood flow volume of the SMA (mL/min)	734.8 ± 312.9	704.4 ± 328.1
RI in OA	0.719 ± 0.097	0.707 ± 0.089
RI in CRA	0.661 ± 0.088	0.644 ± 0.052
RI in SPCA	0.624 ± 0.057	0.580 ± 0.037*

(0.16 mm or 0.20 mm × 40 mm; Seirin Co. Ltd., Shizuoka, Japan). Retrobulbar circulation was measured using CDI at rest prior to treatment and 1 hour later, or after acupuncture.

3. Results and Discussion

3.1. Experiment 1: Effects of LR3 Acupuncture on Upper Limb Circulation [1]. Hemodynamic parameters including blood pressure, heart rate, and blood flow volume in the radial and brachial arteries are summarized in Table 1. Figure 6 illustrates the profile of the percent changes in blood flow volume in the radial and brachial arteries. The blood flow volume in the radial artery decreased significantly during acupuncture ($P < 0.01$), but showed a significant increase at 180 seconds after acupuncture ($P < 0.05$) (Figure 6). In the brachial artery, the blood flow volume also showed a significant increase at 180 seconds after acupuncture ($P < 0.05$) (Figure 6). The physiological mechanisms of decrease and increase blood flow volume in upper limb are presumably related to a peripheral vascular resistance due to an instantaneous increase and decrease in sympathetic tone [1]. The present result suggests that LR3 located on the foot and apart from the upper limb can affect the circulation in the upper limb.

3.2. Experiment 2: Effects of LR3 Acupuncture on Blood Circulation to the Eye and through the SMA. The RI of the SPCA was significantly lower after acupuncture than before ($P < 0.05$; Table 2). However, blood flow volume in the SMA was not significantly changed after acupuncture than before (Table 2). The SPCA is the ocular branches of the OA and it supplies blood to the choroid (Figure 4) [32]. The decrease of the distal vascular resistance in the SPCA that

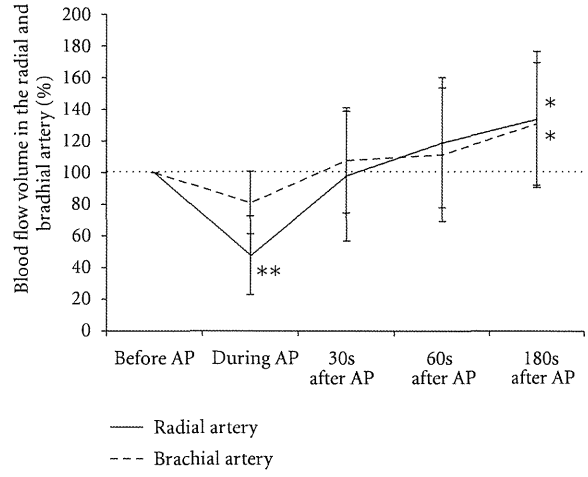

Figure 6: Percent changes in blood flow volume in the radial and brachial arteries before, during, and after acupuncture treatment. Values are presented as a percentage of the pretreatment blood flow. Values represent the mean and SD. AP: acupuncture. $^{*}P < 0.05$, $^{**}P < 0.01$ versus before acupuncture. Modified from [1].

we observed indicates that acupuncture on LR3 results in an increase of the blood flow to the choroid. It has been reported that the blood flow in the eye is controlled by sympathetic and parasympathetic nerves, and it is related with the release of nitric oxide or calcitonin gene-related peptide [33, 34]; it has also been reported that the regulation of regional blood flow by somatic afferent stimulation is based on somatoautonomic reflex mechanisms in the choroidal blood flow of the eyeball [34]. The hemodynamic changes in the SPCA by acupuncture may be related with these

Table 3: Hemodynamic parameters, blood flow volume of the SMA, and resistive index of retrobulbar arteries by acupuncture on ST36. The values represent the mean and SD. $^{*}P < 0.05$, $^{**}P < 0.01$ versus before acupuncture.

Parameters	Acupuncture on ST36	
	Before	After
Systolic blood pressure (mmHg)	121.7 ± 11.8	120.7 ± 10.9
Diastolic blood pressure (mmHg)	77.8 ± 9.4	77.6 ± 7.6
Heart rate (beats/min)	61.9 ± 6.6	61.5 ± 7.4
Blood flow volume of the SMA (mL/min)	549.8 ± 192.2	620.2 ± 188.1*
RI in OA	0.736 ± 0.07	0.728 ± 0.070
RI in CRA	0.617 ± 0.065	0.631 ± 0.043
RI in SPCA	0.600 ± 0.030	0.580 ± 0.06

Table 4: Hemodynamic parameters and resistive index of retrobulbar arteries in control and acupuncture therapy. The values represent the mean and SD. $^{*}P < 0.05$, $^{**}P < 0.01$ versus rest or before acupuncture. $^{\dagger}P < 0.05$, $^{\dagger\dagger}P < 0.01$ versus control. Modified from [2].

Parameters	Control		Acupuncture	
	Rest	After 1 hour	Before	After
Systolic blood pressure (mmHg)	116.4 ± 10.0	119.8 ± 7.6	124.5 ± 12.9	122.6 ± 9.7
Diastolic blood pressure (mmHg)	69.8 ± 6.5	68.6 ± 3.9	74.5 ± 5.4	72.0 ± 2.9
Heart rate (beats/min)	61.5 ± 7.3	60.1 ± 8.1	61.7 ± 8.5	60.3 ± 10.4
RI in OA	0.74 ± 0.04	0.75 ± 0.05	0.74 ± 0.04	0.74 ± 0.04
RI in CRA	0.75 ± 0.09	0.72 ± 0.03	0.72 ± 0.05	0.68 ± 0.04*
RI in SPCA	0.68 ± 0.05	0.68 ± 0.04	0.67 ± 0.04	0.64 ± 0.06*††

mechanisms. The present result suggests that LR3 located on the foot and apart from the eye can affect the circulation in the retrobulbar arteries.

3.3. Experiment 3: Effects of ST36 Acupuncture on Blood Circulation to the Eye and through the SMA. RI in the retrobulbar vessels was not changed by ST36 acupuncture treatment. However, the blood flow volume in the SMA was significantly greater after acupuncture than before ($P < 0.05$; Table 3). Acupuncture on the limbs was also demonstrated to elicit systemic visceral responses via the supraspinal reflexes in animal models [9, 36, 37]. According to several reports, blood flow volume in the SMA increased significantly after stimulation of the lower limbs [9, 36–38]. We speculate that this increase is caused by excitation of the parasympathetic system and inhibition of the sympathetic system via supraspinal reflexes. The present result suggests that ST36 located on the lower limb and apart from the abdomen can affect the circulation in the SMA.

3.4. Experiment 4: Effects of Acupuncture on Retrobulbar Circulation in OAG Patients. RI in the CRA and SPCA were significantly lower after acupuncture than it was before acupuncture treatment (CRA; $P < 0.05$, SPCA; $P < 0.05$; Table 4). RI in the SPCA was also significantly lower after acupuncture than when no treatment was given (SPCA; $P < 0.01$; Table 4). The CRA supplies blood to the retina and SPCA, to the choroid (Figure 4). The decrease of the distal vascular resistance in the CRA and SPCA that we observed indicates that acupuncture results in an increase of the blood flow to the retina and choroid. The possible physiological mechanisms of increase blood flow in eye has already described in the discussion of Experiment 2. The present result suggests that acupuncture can improve the retrobulbar circulation in the patients of OAG with standard medication.

4. Ultrasound and CDI

4.1. Advantage. We focused on the evaluation of CDI by ultrasound. Noninvasive and real-time measure of CDI was applied to assess circulation in organs after acupuncture. The continuous method of CDI was used to assess the brief effects of circulation in the arm (Experiment 1). The simultaneous evaluation by CDI was applied to assess the circulation in two different organs (Experiments 2 and 3). Resistive index measured by CDI is measured in the small vessels as retrobulbar arteries (Experiment 4). Acupuncture affects the autonomic nervous system via the somatic nerves. Invasive evaluation also affects these systems and reflex. Therefore, invasive evaluation might not correctly evaluate the physiological effects of acupuncture therapy. We suggest that real-time and noninvasive hemodynamic measurement as CDI is suitable to measure the physiological effects in humans.

4.2. Limitation. While CDI provides detailed images of blood vessels in real-time, there are limits to the hemodynamic measurements that can be made using this technique. In addition, while CDI is useful for the measurement of blood flow in various vessels in real time, it does not have sufficient resolution to determine the diameter of very small retrobulbar vessels such as OA, CRA, and SPCA. Therefore,

CDI cannot be used to measure blood flow volume in these vessels. However, it can provide an index of vascular resistance such as RI. A decrease in the distal vascular resistance in the small vessels indicates an increase in the blood flow in the distal part of the vessels. Additionally, care must be taken to avoid compression of the eyeball during ultrasound examination. Such compression is likely to cause intraocular pressure elevation and trigger the vagal reflex. Measurement of blood flow in the retrobulbar arteries requires attention to probe maintenance and careful avoidance of pressure on the eyeball [23]. Expert technique is required to obtain reproducible results using CDI. In addition to the limits of CDI resolution, ultrasound waves that strike blood vessels at angles greater than 60° relative to the direction of blood flow result in a large margin of error for CDI measurements. Therefore, it is important to measure blood flow at a Doppler angle of less than 60 degrees [34, 35].

4.3. Further Study. The other methods to assess the physiological changes by acupuncture noninvasively are impedance cardiography and spectral analysis of heart rate variability. Impedance cardiography is a noninvasive monitoring method that allows measurement of the cardiac index based on the changes in thoracic resistance that results from variations in intrathoracic blood flow volume [39, 40]. Spectral analysis of heart rate variability is useful to evaluate the autonomic nervous balance noninvasively [41, 42]. Combined with these measurements, we can clarify the mechanism of increased blood flow volume in several organs in humans. In the future, we would like to explore the efficacy of acupuncture as treatment for various diseases by using diagnostic tools, such as CDI.

5. Conclusion

CDI can noninvasively depict blood vessels in the human body, and can quantitatively evaluate blood flow in real time. Our studies showed the changes of blood flow in the peripheral, mesenteric, and retrobulbar arteries by acupuncture estimated by CDI. This technique is suitable as an evaluation method to consider physiological changes due to acupuncture as blood flow changes.

Conflict of Interests

The authors have no conflict of interests.

Acknowledgments

Experiment 1 was supported by Special Coordination Funds for Promoting Science and Technology from the Japanese Ministry of Education, Culture, Sports, Science and Technology. Experiment 4 was supported by Health and Labour Sciences Research Grants for Clinical Research from the Japanese Ministry of Health, Labour and Welfare.

References

[1] S. Takayama, T. Seki, M. Watanabe et al., "Brief effect of acupuncture on the peripheral arterial system of the upper limb and systemic hemodynamics in humans," *Journal of Alternative and Complementary Medicine*, vol. 16, no. 7, pp. 707–713, 2010.

[2] S. Takayama, T. Seki, T. Nakazawa et al., "Short-term effects of acupuncture on open-angle glaucoma in retrobulbar circulation: additional therapy to standard medication," *Evidence-Based Complementary and Alternative Medicine*, vol. 2011, Article ID 157090, 6 pages, 2011.

[3] S. Takayama, T. Seki, M. Watanabe et al., "Changes of blood flow volume in the superior mesenteric artery and brachial artery with abdominal thermal stimulation," *Evidence-Based Complementary and Alternative Medicine*, vol. 2011, Article ID 214089, 10 pages, 2011.

[4] S. Takayama, T. Seki, N. Sugita et al., "Radial artery hemodynamic changes related to acupuncture," *Explore*, vol. 6, no. 2, pp. 100–105, 2010.

[5] S. Takayama, T. Seki, M. Watanabe et al., "The effect of warming of the abdomen and of herbal medicine on superior mesenteric artery blood flow—a pilot study," *Forschende Komplementarmedizin*, vol. 17, no. 4, pp. 195–201, 2010.

[6] D. Irnich and A. Beyer, "Neurobiological mechanisms of acupuncture analgesia," *Schmerz*, vol. 16, no. 2, pp. 93–102, 2002.

[7] J. G. Lin and W. L. Chen, "Acupuncture analgesia: a review of its mechanisms of actions," *American Journal of Chinese Medicine*, vol. 36, no. 4, pp. 635–645, 2008.

[8] Z. Q. Zhao, "Neural mechanism underlying acupuncture analgesia," *Progress in Neurobiology*, vol. 85, no. 4, pp. 355–375, 2008.

[9] S. Uchida and H. Hotta, "Acupuncture affects regional blood flow in various organs," *Evidence-Based Complementary and Alternative Medicine*, vol. 5, no. 2, pp. 145–151, 2008.

[10] H. Tsuru and K. Kawakita, "Acupuncture on the blood flow of various organs measured simultaneously by colored microspheres in rats," *Evidence-Based Complementary and Alternative Medicine*, vol. 6, no. 1, pp. 77–83, 2009.

[11] E. Haker, H. Egekvist, and P. Bjerring, "Effect of sensory stimulation (acupuncture) on sympathetic and parasympathetic activities in healthy subjects," *Journal of the Autonomic Nervous System*, vol. 79, no. 1, pp. 52–59, 2000.

[12] Y. Syuu, H. Matsubara, T. Kiyooka et al., "Cardiovascular beneficial effects of electroacupuncture at Neiguan (PC-6) acupoint in anesthetized open-chest dog," *Japanese Journal of Physiology*, vol. 51, no. 2, pp. 231–238, 2001.

[13] J. Soga, K. Nishioka, S. Nakamura et al., "Measurement of flow-mediated vasodilation of the brachial artery—a comparison of measurements in the seated and supine positions," *Circulation Journal*, vol. 71, no. 5, pp. 736–740, 2007.

[14] J. Deanfield, A. Donald, C. Ferri et al., "Endothelial function and dysfunction. Part I: methodological issues for assessment in the different vascular beds: a statement by the working group on endothelin and endothelial factors of the European society of hypertension," *Journal of Hypertension*, vol. 23, no. 1, pp. 7–17, 2005.

[15] J. Kjeldsen and O. B. Schaffalitzky de Muckadell, "Assessment of disease severity and activity in inflammatory bowel disease," *Scandinavian Journal of Gastroenterology*, vol. 28, no. 1, pp. 1–9, 1993.

[16] M. J. Perko, "Duplex ultrasound for assessment of superior mesenteric artery blood flow," *European Journal of Vascular and Endovascular Surgery*, vol. 21, no. 2, pp. 106–117, 2001.

[17] G. L. Moneta, D. C. Taylor, W. S. Helton, M. W. Mulholland, and D. E. Strandness, "Duplex ultrasound measurement of postprandial intestinal blood flow: effect of meal composition," *Gastroenterology*, vol. 95, no. 5, pp. 1294–1301, 1988.

[18] A. Erden, T. Cumhur, and T. Ölçer, "Superior mesenteric artery Doppler waveform changes in response to inflammation of the ileocecal region," *Abdominal Imaging*, vol. 22, no. 5, pp. 483–488, 1997.

[19] M. F. Byrne, M. A. Farrell, S. Abass et al., "Assessment of Crohn's disease activity by Doppler sonography of the superior mesenteric artery, clinical evaluation and the Crohn's disease activity index: a prospective study," *Clinical Radiology*, vol. 56, no. 12, pp. 973–978, 2001.

[20] A. Sigirci, T. Baysal, R. Kutlu et al., "Doppler sonography of the inferior and superior mesenteric arteries in ulcerative colitis," *Journal of Clinical Ultrasound*, vol. 29, no. 3, pp. 130–139, 2001.

[21] C. R. Deane and H. S. Markus, "Colour velocity flow measurement: in vitro validation and application to human carotid arteries," *Ultrasound in Medicine and Biology*, vol. 23, no. 3, pp. 447–452, 1997.

[22] U. Gembruch, "Assessment of the fetal circulatory state in uteroplacental insufficiency by Doppler ultrasound: which vessels are the most practicable?" *Ultrasound in Obstetrics and Gynecology*, vol. 8, no. 2, pp. 77–81, 1996.

[23] E. T. Matthiessen, O. Zeitz, G. Richard, and M. Klemm, "Reproducibility of blood flow velocity measurements using colour decoded Doppler imaging," *Eye*, vol. 18, no. 4, pp. 400–405, 2004.

[24] D. Bensky and J. O'Connor, *Acupuncture a Comprehensive Text*, Eastland Press, Seattle, Wash, USA, 1981.

[25] M. Giovanni, *The Moundations of Chinese Medicine*, Churchill Livingstone, Philadelphia, Pa, USA, 1989.

[26] Y. Yamazaki and S. M. Drance, "The relationship between progression of visual field defects and retrobulbar circulation in patients with glaucoma," *American Journal of Ophthalmology*, vol. 124, no. 3, pp. 287–295, 1997.

[27] I. Stalmans, A. Harris, S. Fieuws et al., "Color Doppler imaging and ocular pulse amplitude in glaucomatous and healthy eyes," *European Journal of Ophthalmology*, vol. 19, no. 4, pp. 580–587, 2009.

[28] M. Satilmis, S. Orgül, B. Doubler, and J. Flammer, "Rate of progression of glaucoma correlates with retrobulbar circulation and intraocular pressure," *American Journal of Ophthalmology*, vol. 135, no. 5, pp. 664–669, 2003.

[29] J. Schumann, S. Orgül, K. Gugleta, B. Dubler, and J. Flammer, "Interocular difference in progression of glaucoma correlates with interocular differences in retrobulbar circulation," *American Journal of Ophthalmology*, vol. 129, no. 6, pp. 728–733, 2000.

[30] R. W. Gill, "Measurement of blood flow by ultrasound: accuracy and sources of error," *Ultrasound in Medicine and Biology*, vol. 11, no. 4, pp. 625–641, 1985.

[31] F. Van Bel, P. H. T. Van Zwieten, G. L. Guit, and J. Schipper, "Superior mesenteric artery blood flow velocity and estimated volume flow: duplex Doppler US study of preterm and term neonates," *Radiology*, vol. 174, no. 1, pp. 165–169, 1990.

[32] K. Mayumi, "Aiming at a wide range of applications from preventive medicine to treatment," *Innervision*, vol. 21, no. 4, pp. 20–21, 2006.

[33] O. Takashi, "Measurement of minimal changes in blood vessels and its application," *Journal of Clinical Echocardiography*, vol. 7, no. 11, pp. 936–941, 2006.

[34] P. N. Burns and C. C. Jaffe, "Quamtitative flow measurements with Doppler ultrasound: techniques, accuracy, and limitations," *Radiologic Clinics of North America*, vol. 23, no. 4, pp. 641–657, 1985.

[35] K. J. W. Taylor and S. Holland, "Doppler US. Part I. Basic principles, instrumentation, and pitfalls," *Radiology*, vol. 174, no. 2, pp. 297–307, 1990.

[36] A. Sato, Y. Sato, A. Suzuki, and S. Uchida, "Reflex modulation of catecholamine secretion and adrenal sympathetic nerve activity by acupuncture-like stimulation in anesthetized rat," *Japanese Journal of Physiology*, vol. 46, no. 5, pp. 411–421, 1996.

[37] E. Noguchi, "Mechanism of reflex regulation of the gastroduodenal function by acupuncture," *Evidence-Based Complementary and Alternative Medicine*, vol. 5, no. 3, pp. 251–256, 2008.

[38] M. Watanabe, S. Takayama, T. Seki et al., "Haemodynamic changes in the superior mesenteric artery induced by acupuncture stimulation on the lower limbs," *Evidence-Based Complementary and Alternative Medicine*. In press.

[39] A. C. Perrino, A. Lippman, C. Ariyan, T. Z. O'Connor, and M. Luther, "Intraoperative cardiac output monitoring: comparison of impedance cardiography and thermodilution," *Journal of Cardiothoracic and Vascular Anesthesia*, vol. 8, no. 1, pp. 24–29, 1994.

[40] N. M. Albert, M. D. Hail, J. Li, and J. B. Young, "Equivalence of the bioimpedance and thermodilution methods in measuring cardiac output in hospitalized patients with advanced, decompensated chronic heart failure," *American Journal of Critical Care*, vol. 13, no. 6, pp. 469–479, 2004.

[41] S. Lee, Y. Chae, S. N. Kim et al., "Short term effects by acupuncture to SP3 on the autonomic blood flow control," *Neurological Research*, vol. 32, no. 1, pp. S37–S42, 2010.

[42] J. H. Lee, K. H. Kim, J. W. Hong, W. C. Lee, and S. Koo, "Comparison of electroacupuncture frequency-related effects on heart rate variability in healthy volunteers: a randomized clinical trial," *Journal of Acupuncture and Meridian Studies*, vol. 4, no. 2, pp. 107–115, 2011.